

POLITECNICO DI TORINO

Corso di Laurea Magistrale in Ingegneria Elettrica



Tesi di Laurea Magistrale

NVH system-level modelling for Induction Machine Electric Drives

Supervisors

Prof. Michele PASTORELLI

Prof. Johan GYSELINCK

Candidate

Giulia IETRO

Luglio 2020

Abstract

Nowadays, the market for electric vehicles (EV) is rising and to meet this demand NVH (Noise, Vibration and Harshness) engineers are challenged to define and refine the sound and comfort of the vehicle, without hindering its efficiency.

This thesis tries to provide a useful tool for electric motor designers, since electrical machines are among the main sources of NVH in an EV.

A fast induction machine (IM) system-level model able to capture spatial force effect in the air-gap is developed. The IM model is constructed using the early-stage machine-design Simcenter SPEED, by a fast, semi-analytical parameter extraction approach. The model is coupled with Noise App, a Python-based application developed by the Engineering Service department of Siemens SW, Leuven. Knowing the air-gap spatial forces distribution, *Noise App* allows to estimate the vibration displacement and the acoustic noise.

In a few moments and with low computational power, the electrical machine designer will be so aware of how the construction choices impact on the production of vibration and noise, will be able to adjust the design in order to minimize NVH.

*Thanks to the beloved people met during those years.
A special thanks to my supervisors Prof. Michele Pastorelli, Prof. Johan
Gyselinck, Dr. Ing. Yves Mollet and Sebastian Ciceo for all the help I've received
during these months of work.*

Contents

List of Tables	VII
List of Figures	VIII
1 Introduction	1
1.1 Induction Machine in Electric Vehicles	1
1.2 Context of the work	2
1.3 Aim	2
1.3.1 System-Level Model	5
1.3.2 Results Post-Processing	6
1.4 SPEED Electrical Machine Design Software	7
1.4.1 PC-IMD	7
1.4.2 Finite Element Analysis - GoFER and PC-FEA	8
1.4.3 Kyburtz eRod Induction Motor Design	8
1.5 Working Principle of an Induction motor	11
2 Induction Machine system-level model	15
2.1 Introduction	15
2.2 Electrical and Magnetic Equations	17
2.3 Equations of Transformation	20
2.4 Rotor Reference Frame	21
2.5 Rotor Flux Reference Frame	23
2.6 Simulink Implementation	26
2.7 Inclusion of the saturating effect of the magnetizing inductance	27
2.8 Coupling Simulink Model with FEA	29
3 Stator Magnetomotive Force	30
3.1 Characterisation of a winding	30
3.2 Winding functions definition	32
3.3 Analytical computation of Radial Magnetic Induction in MATLAB	33
3.4 Testing the Stator MMF	34

3.4.1	Single Load Point Finite Element Analysis	36
4	Rotor Magnetomotive Force	40
4.1	Current distribution in rotor bars	40
4.2	A winding function approach	41
4.3	Winding Theory - Ratio between Stator and Rotor	42
4.4	Testing the Rotor MMF	44
5	Airgap Permeance	47
5.1	Slotting Effect	49
5.1.1	Modified Air-gap width	49
5.2	Saturation	51
6	Noise and Vibrations	56
6.1	Noise App: Introduction	56
6.2	Noise App Inputs	57
6.3	Results: Constant RPM simulation	58
6.4	Run-Up Results	60
7	Conclusions	62
	Bibliography	63

List of Tables

1.1	DG112M-4 FL - Name plate data	9
1.2	Geometrical data of Simrod e-motor	10
1.3	Stator and rotor equivalent circuit parameters	13
6.1	Noise App results: Mode and Frequencies	60

List of Figures

1.1	Kyburz eRod	3
1.2	Work Flow	4
1.3	Kyburz eRod - Induction Motor	9
1.4	Kyburz eRod - PC-IMD Winding Editor	10
1.5	Kyburz eRod - PC-IMD Equivalent circuit	11
1.6	Stator and Rotor equivalent representation	13
1.7	Induction Motor Equivalent Circuit	14
2.1	Symmetrical Induction Machine: Stator and rotor windings	16
2.2	d,q axes in a three-phase induction motor	20
2.3	dq - Induction Motor Equivalent Circuit	22
2.4	Rotor Reference Frame	22
2.5	IM model in rotor reference frame - Simulink implementation	23
2.6	Rotor Flux Reference Frame	24
2.7	IM model in rotor flux reference frame - Simulink implementation	26
2.8	System-level model	27
2.9	Modified Induction Motor model	28
2.10	Magnetizing Effect of Saturation Inductance	28
2.11	Flux linkages	29
3.1	PC-IMD Winding Editor	31
3.2	Winding Editor - Export winding	32
3.3	Winding Function - Phase A	33
3.4	Winding Layout - All Phases	34
3.5	Stator Magnetomotive Force	35
3.6	Simplified Geometry for testing stator MMF	36
3.7	FEA results: Zone paint: Vector Potential and Magnetic flux density, Equipotential lines: Vector Potential	37
3.8	Radial and Tangential Magnetic Induction in the air-gap	38
3.9	Comparison between FEA and analytical results	38

3.10	Comparison between FEA and analytical results:different electrical positions	39
4.1	Squirrel Cage Rotor	41
4.2	Rotor MMF: a winding function approach	41
4.3	Winding functions of 4 loops (12 cages rotor)	42
4.4	Simplified Geometry: Testing Rotor MMF	44
4.5	Comparison between FEA and analytical results	45
4.6	Comparison between FEA and analytical results: Different rotor positions	46
5.1	B-field with Ideal Permeance	48
5.2	Computation of stator slotting function	49
5.3	Modified air-gap depth	50
5.4	Air-gap Permeance - Including slotting effect	51
5.5	Radial Magnetic Inductance - Including slotting effect	52
5.6	Comparison between PC-FEA Magnetic Induction and Stator Magnetomotive Force computed analytically, for a defined value of stator current amplitude	53
5.7	Virtual Permeance	54
5.8	Saturation Constant	54
6.1	Structural and acoustic model- Noise App	56
6.2	Radial Magnetic induction: air-gap distribution during a complete mechanical rotation	58
6.3	Maxwell stress-tensor: air-gap distribution during a complete mechanical rotation	58
6.4	Maxwell stress-tensor distribution in the airgap	59
6.5	Noise App results: Constant RPM simulation. Left: Vibration displacement vs. frequency. Right: Sound Pressure vs. frequency .	60
6.6	Noise App results: Run-Up test. (Up) Result obtained including saturation effect in air-gap permeance computation. (Down) Result obtained neglecting saturation effect in air-gap permeance computation.	61

Chapter 1

Introduction

1.1 Induction Machine in Electric Vehicles

Electric motors and generators are widely used in the vehicles, even before the fast development of hybrid electric vehicles (HEV) and electric vehicles (EV).

State of the art drive trains for Electric Vehicles (EVs) are often equipped with induction motors (IM) or permanent magnet (PM) synchronous motors [1]. Despite induction machine is one of the oldest motor technologies, among all passengers EVs/HEVs, a limited number of models use IMs.

Around 90% of pure battery electric vehicle models currently use rare earth permanent magnet synchronous motors (PMSMs) in the drivetrain. The use of rare earth PMSMs allows vehicle manufacturers to have higher torque density and efficiency compared to induction motors, especially at lower revolutions. Among PM motors, both surface-mounted PM (SPM) and interior PM (IPM) types are adopted for traction. Synchronous PM drives require a custom control algorithm, when flux-weakening operation is required over a wide speed range, as it is the case of traction. The motor magnetic model must be consistently identified for accurate control, with the experimental identification tests that are considered cumbersome if compared to the standard ones, usual for IMs. The recent issue of the rare-earth magnets price volatility is seriously questioning the adoption of PM motor drives. In this context, Induction Machines appear good alternatives to PMSMs.

TESLA Roadster Sport, General Motors Company for Chevy Spark [2], and the more recent Audi e-tron are examples of Electric Vehicles equipped with Induction Machines. IM drives are adopted for their ruggedness and universal availability. For what concerns control, field-oriented vector control of IMs is considered a standard, industrially. Due to the field weakening capabilities of induction machines, inverter ratings and costs appear to be lower, especially for high performance drives. Moreover, IMs are naturally de-excited in case of inverter fault and this is very

welcome among car manufacturers, for safety reasons. Finally, asynchronous motor is efficient, of simple construction and the absence of slip rings and brushes requires low maintenance.

For the above reasons, with a view to greater penetration into the electric vehicle industry in the coming years, studying and characterizing the performance of the asynchronous motor is of crucial importance. This work seeks to provide additional tools during the IM design phase; the results of which are produced easily and in a short time.

1.2 Context of the work

The automotive industry is undergoing a radical transformation, and most car manufacturers agree that the next 10 years will bring more change than the previous two decades, with a substantial integration of electric and hybrid solutions alongside conventional combustion vehicles. For that precise reason, some companies like Siemens are willing to answer to this increasing demand by providing new digital solutions. Siemens PLM is a company specialized in software development, mainly in the product lifecycle management field. Partially, this work takes place within the framework of the European project OBELICS (Optimization of scalaBle rEaltime modeLs and functIonal testing for e-drive ConceptS) [3]. Before EVs mass deployment become a reality, real operational performance, safety, reliability, durability and affordability of EVs should attain at least the same level as conventional vehicles. In this context, the OBELICS project address the urgent need for new tools to enable the multi-level modelling and testing of EV and their components in order to deliver more efficient vehicle designs faster while supporting modularity to enable mass production and hence improved affordability.

Siemens PLM software in Leuven took part of the project in collaboration with the Swiss company Kyburz. With its open design, Kyburz eRod (Figure 1.1) lends itself well to be easily characterized and improved. Kyburz eRod is equipped with a squirrel-cage induction machine.

At the same time, this work has been carried out in collaboration with the Engineering Service Division of Siemens PLM. In this department, RD engineers are developing a fast e-machine NVH post-processing tool called "Noise App". Knowing the distribution of forces in the air-gap, Noise App performs structural and acoustic analysis and estimates noise and vibration displacement.

1.3 Aim

The market for electric vehicles is rising and to meet this demand NVH engineers are challenged to define and refine the sound and comfort of the vehicle without



Figure 1.1: Kyburz eRod

hindering its efficiency. Electrical machines are among the main contributors to noise and vibration production. To reduce NVH, an intervention can take place in two specific moments: during and after the design process. With the help of low-computational cost reduced-order models, the designer is able to know in advance the impact of design choices, having the chance to properly design motors, aiming to minimize NVH. Once the design process is over, it is possible to define NVH-optimized control strategies.

This work lies within the first of the two cases highlighted above: in the following chapters, a fast system-level model of an Induction machine able to estimate radial forces in the air-gap is developed. The model is able to catch motor transients and the influence of drives coupled with it (inverters, sensors, control strategies). It is then coupled with a fast e-machine NVH post-processing tool called "Noise App", developed by Siemens Leuven Engineering Service department that predicts radiated noise based on motor parameters and point source model.

Because of the practical utility of the tool, the electromagnetic model is linked to the electrical machines design software Simcenter SPEED (described in detail in Section 1.4) . In the design software, the designer can specify all the design choices (such as geometry, materials, electrical parameters). SPEED computes, pure analytically the quantities that characterised the defined design together with the performances of the motor at specified operating points. The information needed for running the system-level model are extracted and radial forces in the air-gap computed. The results of the simulation will be post-processed by Noise App, that will perform NVH analysis.

Figure 1.2 gives a quick overview of the workflow. It will be discussed in more detail in Sections 1.3.1 and 1.3.2 and in dedicated chapters. Note that the model consists mainly of two parts: *System-Level Model* presented in Section 1.3.1 (block 2 of Figure 1.2) and *Result Post-Processing* in Section 1.3.2 (blocks 3, 4, 5, 6 of

Figure 1.2).

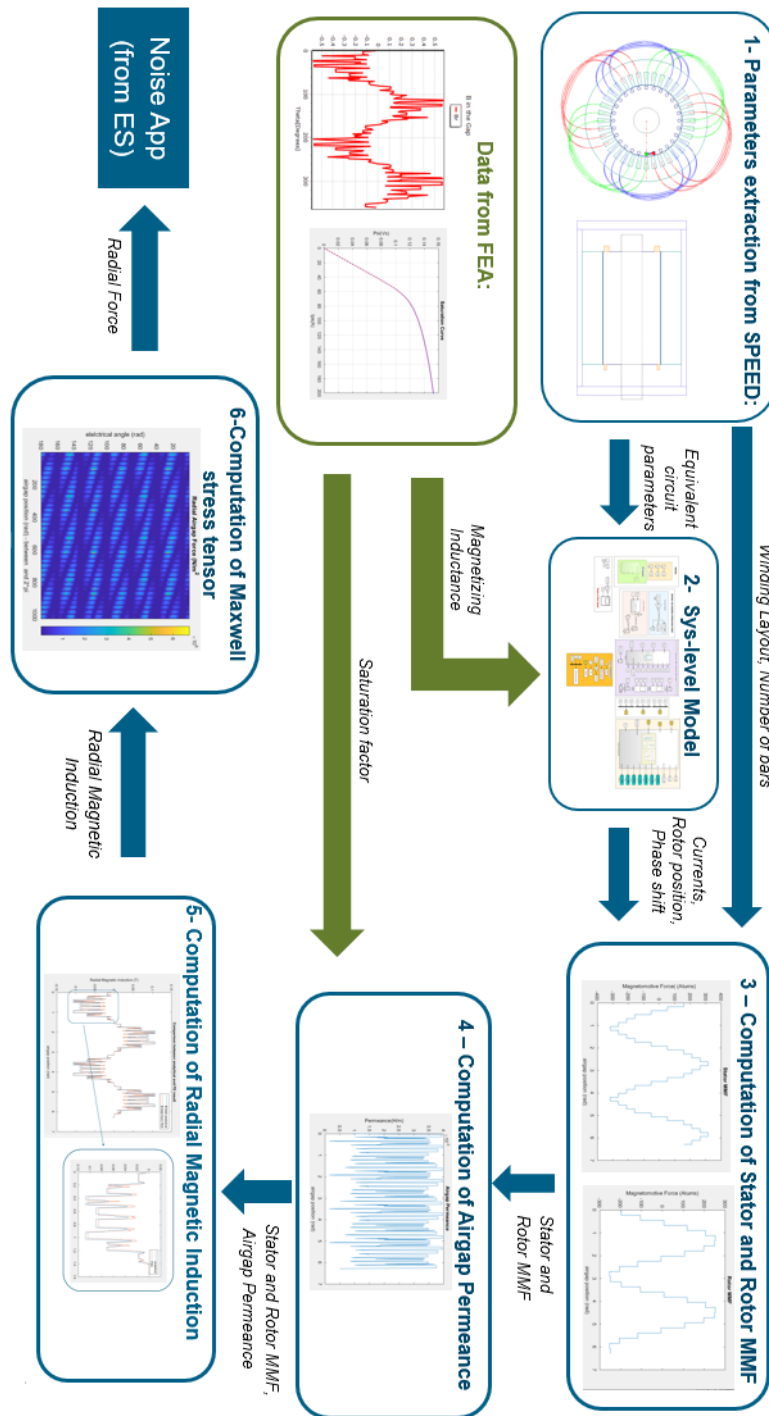


Figure 1.2: Work Flow

1.3.1 System-Level Model

A dynamic model of the induction machine is built (block *2-Sys-level Model* in Figure 1.2). In order to simplify the IM equations, a rotating d,q frame is preferred to a three-phase reference (Section 2.3). Machine equations in d,q rotor and rotor-flux reference frame are discussed in details in Sections 2.4 and 2.5. The user can choose between the two references, to observe different quantities or to couple the motor block with different kind of controllers.

Firstly, d,q equivalent circuit quantities (resistances and inductances) are assumed to be constant values. In Section 2.7, exploiting the No-Load PC-FEA test results, the saturating effect of magnetizing inductance is modelled. In order to include this last effect, IM models in d,q-reference frames are slightly modified.

The dynamic-model receives as inputs:

- *Equivalent circuit parameters computed in PC-IMD (Section 1.4)*

After specifying the design choices in SPEED's PC-IMD (Section 1.4), a design sheet collecting a wide range of performance parameters is generated. The data concerning the T-equivalent circuit parameters (stator and rotor resistances and reactances and the magnetizing reactance) are imported in the dynamic model.

- *Information regarding the operating point*

The operating point is defined setting the desired rotor speed or load torque, together with the choice of the drive that feeds the machine.

If a sinusoidal voltage source is considered, voltage amplitude and frequency should be specified (either manually or imported by SPEED's design sheet). Moreover, a simple first-order current controller is implemented. In this case, the user should specify the desired values of stator current.

It is also possible to perform a run-up test: rotor speed range and test time should be specified manually. Torque-vs.-speed machine characteristic may be computed.

During the simulation, stator and rotor currents, together with the electromagnetic torque are calculated and machine transients are properly described.

The model includes also a small section dedicated to losses computation. It should be considered as a first approximation, since iron losses are neglected (no iron resistance appears in the equivalent circuit at this stage of the work). It was mainly used to validate the coupling between the system-level model and the electrical machine software design SPEED.

The outputs of the system-level model are:

- Instantaneous values of three-phases stator currents;
- Rotor position (electrical degrees);
- Rms values of stator and rotor currents and phase shift between stator and rotor phasors.

The dynamic model was developed in Simulink. For different Induction machines and choosing few operating points, the homemade blocks (IM in d,q rotor and rotor-flux frame) were validated comparing currents and torque profile with the output of Amesim squirrel-cage induction motor models. Amesim is a commercial simulation software developed by Siemens for the modelling and analysis of multi-domain system. The idea was to reproduce the existing blocks (for educational purposes only) and to integrate them with the work of this thesis (and other future works in the same field), in order to transfer on a commercial software a fast system-level model able to estimate the impact of NVH during the electrical machine design process.

1.3.2 Results Post-Processing

The estimation of radial forces in the air-gap requires that dynamic-simulation results should be post-processed. Referring to Figure 1.2, this part concerns blocks:

- 3 - *Computation of stator and rotor magnetomotive force;*
- 4 - *Computation of airgap permeance;*
- 5 - *Computation of radial magnetic Induction;*
- 6 - *Computation of radial force pressure (via Maxwell stress tensor).*

Results post-processing was performed in MATLAB. Specyfing the machine design file (defined by PC-IMD, Section 1.4), after running the dynamic simulation (in Simulink) airgap forces will be computed in MATLAB script. It has the following structure:

- Processing of the data obtained from the system-level model and machine design choices defined in SPEED (i.e. winding layout, number of rotor bars, motor dimensions such as air-gap width, stator and rotor slot openings;
- Computation of stator winding functions. Definition of stator magnetomotive force;

- Distribution of the current in rotor bars. Definition of number-of-rotor-bars winding functions (using the same approach of the stator). Computation of rotor magneto motive force.
- Computation of the air-gap permeance, taking into account the effect of the slots and the saturation of the material. Comparison between analytical approximation with Finite element simulations and upload of the analytical model with the creation of Look-up-tables collecting the correction factors per space harmonics in order to have the best fitting with FEA.
- Computation of radial force pressure (via Maxwell stress tensor), neglecting the contribution of tangential component of the Magnetic Induction. This will be the input of NoiseApp.

1.4 SPEED Electrical Machine Design Software

Originally developed in the Department of Electronics and Electrical Engineering at the University of Glasgow, UK, Simcenter SPEED primary focus is in the technology of calculating electrical machines.

1.4.1 PC-IMD

Several types of electrical machines can be designed in SPEED environment (Brushless PM machines and drives, induction motors, switched reluctance motors, wound-field AC and DC commutator motors, axial flux machines).

PC-IMD is intended for designing and calculating induction motors. It is based on classical theory of the induction motor [4]. The performance calculation includes virtually all the electrical and electromagnetic performance of the machine: for example, torque, efficiency, current, power factor and torque. Electrical parameters such as winding parameters with resistances and inductances are presented in detail. There are many dimensional and mechanical parameters including weights and inertias, and a comprehensive set of thermal calculations is included. Magnetic flux-densities are given in various parts of the machine, together with a detailed breakdown of losses.

To make the motor design fast and efficient, PC-IMD has an outline editor for modifying the cross-section and other motor dimensions. There is a template editor for electrical parameters, drive parameters and several other inputs. A winding editor is included for displaying the winding layout. PC-IMD also includes a material database for steels. The performance calculation or analysis is either at a single operating point, or over a whole torque/speed range. It includes a time-stepping model of the drive, so that transient performances can be studied (current,

speed and torque waveforms are obtained). The software is able to compute, pure analytically, the parameters of the equivalent circuits, losses, thermal measurements in steady state. There is a design sheet containing a wide range of performance parameters including the dimensions, and details of the winding and the drive. Moreover, in PC-IMD a scripting tool can be used to automate many processes, create new algorithms or processes not already embedded in the program and to interface PC-IMD to other software.

1.4.2 Finite Element Analysis - GoFER and PC-FEA

Finite-element software is often used in support of the design process, as an auxiliary tool for electromagnetic, thermal, or structural analysis [5]. Typically, FE program are slow, both in the interface, in the solution and in the processing of the results. PC-IMD has an efficient link to Simcenter SPEED's own finite-element program PC-FEA. The link is called a GoFER (Go to finite-elements and return) and it uses the GDF (Geometry Definition File) editor, which can also provide links to other finite-element programs. The PC-FEA link is particularly useful because of its speed. Adjusting few values that define the operating points, the user can easily perform FE analysis.

Following, GoFER [6] options for setting up the finite-element calculation used for the purpose of this work are presented:

- Single load point analysis: shows the distribution of air-gap flux density at a particular rotor position and a particular load;
- No-Load ranging: calculates the no-load flux linkage of a phase winding, over a range of current. Used for checking the no-load saturation curve computed analytically in PC-IMD.
- On-load rotate: performs multiple FE analysis of the specified solution domain on-load. The rotor complete a full rotation, in a specified number of steps.

1.4.3 Kyburtz eRod Induction Motor Design

As part of the European project OBELICS (Section 1.2), one of the objectives of this work is to contribute to a multi-level modelling and testing of Kyburtz eRod. For this reason, with the available data, an attempt was made to design the induction machine used in the electric vehicle (Figure 1.3) subject of study.

Kyburz eRod is equipped with a 4 poles induction machine. The data from the name plate are collected in Table 1.1:

In PC-IMD Outline Editor the geometrical data concerning the cross section and



Figure 1.3: Kyburz eRod - Induction Motor

	Max. Torque	Rated Power	Max. Speed
Speed	2460 rpm	5140 rpm	8000 rpm
Torque	100 Nm	28 Nm	12 Nm
Power	26 kW	15 kW	10 kW
Voltage	60 V	60 V	60 V
Frequency	86 Hz	178 Hz	273 Hz
Duty Cycle	S2 - 5 min	S2 - 30 min	S2 - 30 min

Table 1.1: DG112M-4 FL - Name plate data

and the axial measures are entered. This is merely an approximation, as this data was not provided by the manufacturer but measured if accessible. There is almost no information about the rotor. In the future it will be cut in the axial direction to get more information about the shape and size of the rotor slots. Similarly, the stator windings layout has been estimated without being able to remove the windings, so there's no assurance that it's actually correct. However, it was decided to refer the results of this work to this approximate model, precisely in order to proceed towards a wider characterization of the Simrod model.

Table 1.2 presents few geometrical data of the Kyburz eRod Induction motor. Figure 1.4 shows the cross section of the induction motor together with the winding layout of the three stator phases.

Poles	4
Slots	36
Rotor bars	28
Gap	0.35 mm
Shaft radius	18.5 mm
Rotor radius	51 mm
Stator outer radius	87.4 mm
Stack length	200 mm

Table 1.2: Geometrical data of Simrod e-motor

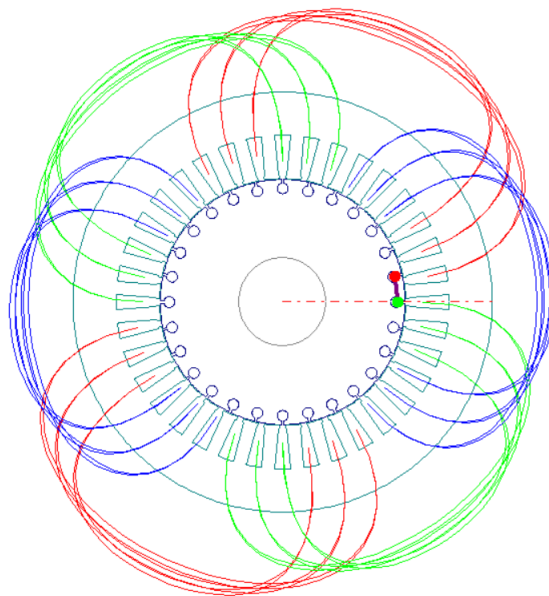


Figure 1.4: Kyburz eRod - PC-IMD Winding Editor

Moreover in Figure 1.5 the T-equivalent circuit is shown (for the operating point: rated power, Table 1.1). Specifying the design choices, setting the electrical parameters and performing steady-state analysis it is easily produced in PC-IMD.

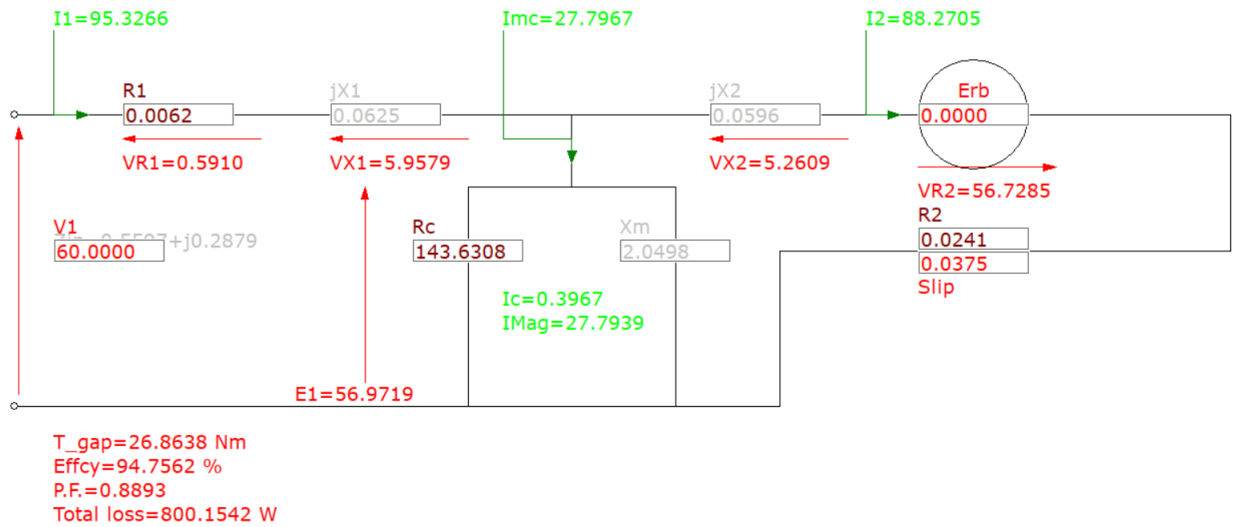


Figure 1.5: Kyburz eRod - PC-IMD Equivalent circuit

1.5 Working Principle of an Induction motor

The aim of this section is to present the working principle of an induction motor and to characterise the T - equivalent circuit that, in Chapter 2, will be used as the starting point for building the dynamic IM model.

An induction machine consists in two main parts:

- Magnetic core: Stator and rotor ferromagnetic cores are realised with laminated steel and are separated by an airgap;
- Windings: distributed in stator and rotor slots. Usually, the stator is equipped with three-phase distributed winding of copper wire. Each coil presents two main parts:
 - *active part* of the winding: inserted in the stator slots and responsible for the production of the magnetic field in the air-gap;
 - *frontal connection*: closes the winding.

Stator winding terminals are linked to an external connection box: delta or star connection are possible. Concerning the squirrel cage rotor: conducting bars, often realized by means of aluminium die cast, are placed in the slots. Rotor bars are short circuited at both ends by means of conducting end-rings.

Induction machines, also known as Asynchronous motors, exploit the rotating magnetic field produced by a statoric polyphase winding when fed with polyphase a.c. currents. The speed of the stator rotating magnetic field

$$\omega_s = \frac{2\pi f}{p} \quad (1.1)$$

where f is the stator current frequency and p is the number of pole pairs, is called *synchronous speed*. The rotating magnetic field induces a system of electromotive forces and current in a rotoric polyphase winding. Rotor e.m.f has a different angular frequency from that of the stator (synchronous speed). Induced rotor e.m.f and currents have frequency equal to sf , where s is the slip. The slip is defined as the relative difference between synchronous and rotor speed:

$$s = \frac{\omega_s - \omega_r}{\omega_s} \quad (1.2)$$

where $\omega_R = \Omega p$ is the electrical pulsation, if the rotor is moving with mechanical speed Ω . The interaction between rotating magnetic field and the induced rotor currents produces the electromagnetic torque. The rotating magnetic field produced by the rotor is synchronous with the rotating magnetic field produced by the stator, thus a continuous torque (Equation 1.4) can be generated. Torque is not zero only for rotor speeds different from synchronous speed. The electromagnetic torque tends to synchronise the rotor with the rotating magnetic field that rotates at synchronous speed. The working principle is therefore based on the electromagnetic induction (*induction machine*). Moreover, in order to generate torque the rotor speed must be different from the synchronous speed (*asynchronous machine*).

Under symmetrical and balanced supply, a first equivalent circuit can be proposed (Figure 1.6). It exploits the analogy between an IM and a transformer, where stator is the primary and rotor the secondary. The machine is like a rotating transformer with ratio, between stator and rotor, of:

$$t = \frac{E_s}{E_{r1}} = \frac{N_s^*}{N_r^*} \quad (1.3)$$

Where:

E_s = e.m.f. produced by stator windings;

E_r = e.m.f induced in rotor windings;

N_s = stator equivalent number of turns;

N_r = rotor equivalent number of turns.

In Figure 1.6, the induction machine is represented as a transformer where stator (primary) and rotor (secondary) equivalent circuits have different frequencies. The parameters that appear in that representation are presented Table 1.3.

Concerning the physical meaning of inductances:

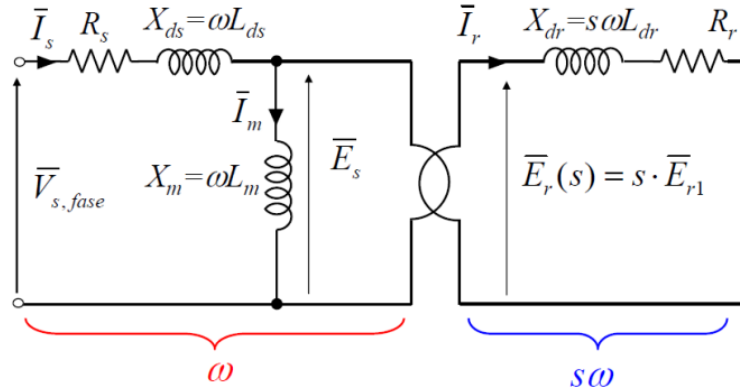


Figure 1.6: Stator and Rotor equivalent representation

Stator Equivalent Circuit	Rotor Equivalent Circuit
$V_{s,phase}$ = stator phase voltage;	
I_s = stator phase current;	I_r = rotor phase current;
E_s = stator phase induced e.m.f.;	E_r = rotor phase induced e.m.f.;
R_s = stator phase resistance;	R_r = rotor phase resistance;
L_{ds} = stator phase leakage inductance;	L_{dr} = rotor phase leakage inductance;
L_m = magnetizing inductance;	
$\omega = 2 \cdot \pi \cdot f$: is the stator angular frequency;	$s \cdot \omega$ = rotor angular frequency;

Table 1.3: Stator and rotor equivalent circuit parameters

- The *leakage inductances* L_{ds} and L_{dr} are related to stator and rotor leakage fluxes (i.e.the fluxes that don't cross the air-gap).
- The *magnetizing inductance* L_m takes into account the presence of the air-gap, and the difference of the magnetic reluctance between the air-gap and the iron core.

It is necessary to modify the equivalent circuit to have stator and rotor at the same frequency. Rotor quantities are divided by the slip: the rotor e.m.f becomes equal to E_s and the rotor leakage reactance X_{ds} presents the stator frequency. Figure 1.7 shows the equivalent T-circuit, where all the rotor quantities are referred to the stator frequency. The fictitious value of rotor resistance $\frac{R'_r}{s}$ takes into account all the power transmitted from stator to rotor. According to the convention shown in the equivalent T-circuit in Figure 1.7 the electromagnetic has the following

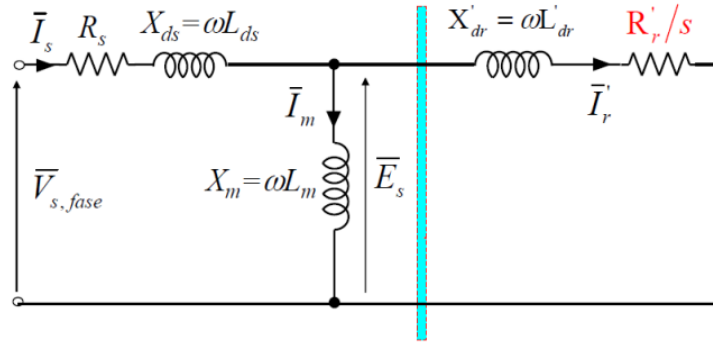


Figure 1.7: Induction Motor Equivalent Circuit

expression:

$$T_m = \frac{3 \cdot \frac{R'_r}{s} \cdot I_r^2}{\omega_s} = \frac{P_t}{\omega_s} [Nm] \quad (1.4)$$

where P_t is the electrical power transmitted from stator to rotor.

Chapter 2

Induction Machine system-level model

In this chapter, a dynamic model of an induction is developed.

Firstly, three-phase electrical and magnetic machine equations are presented (Section 2.2) and briefly, the meaning of the resistances and inductances appearing in the formula is discussed.

Secondly, after a description of the equation of transformation (Section 2.3), machine equations are written in an arbitrary reference frame.

The equations may be expressed in any reference frame by appropriate assignment of the reference-frame speed in the arbitrary reference-frame voltage equations. Although the stationary reference frame, the reference frame fixed in the rotor, and the synchronously rotating reference frame are most frequently used [7].

For this reason, and to satisfy the specifications of different controllers, the dynamic model of the induction motor was developed in two reference frame. Machine equations in rotor frame and in rotor flux reference frame are discussed in detail in Sections 2.4 and 2.5.

2.1 Introduction

In this section, a dynamic model of a Induction Machine is discussed. The model is based on the following assumptions:

- Three-phase induction machine with stator and rotor windings having N_S , N_R equivalent number of turns.
- Only the effects related to the fundamental spatial harmonic of the magnetic induction in the air-gap are taken into account

- One pole pair, symmetrical Induction Machine.
- Constant air-gap depth.
- No magnetic saturation.
- The stator has three identical, sinusoidally distribute windings, displaced 120° , with N_S equivalent number of turns and resistance R_S . The rotor windings will be also be considered as three identical sinusoidally distributed windings, displaced 120° with N_R 2.1 equivalent turns and resistance R_R . [7]

The following calculations refer to an ideal double-fed wounded-rotor Induction Machine (currents are injected in both stator and rotor). The case of Squirrel Cage Induction Machines will be discussed as particular application of the described methodology.

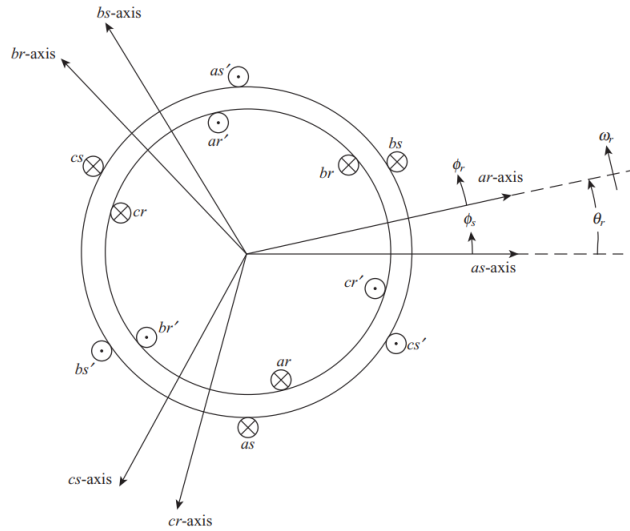


Figure 2.1: Symmetrical Induction Machine: Stator and rotor windings

Note that these restrictive hypothesis, will be gradually modified. Indeed, in the following chapters stator and rotor magnetomotive forces will be computed considering not only the fundamental harmonic, but the real distribution respectively of the windings and the bars in the gap. Moreover, the air-gap depth won't be considered constant, but the presence of stator and rotor slot openings will be taken in account and a modified air-gap depth. Finally, also the effect of yokes and teeth saturation will be considered thanks to the results of Finite Element analysis.

2.2 Electrical and Magnetic Equations

The stator and rotor are supposed to be powered separately. No assumptions have been made about the connection type of the windings. The electrical and magnetic equations of the asynchronous machine [8] are defined in Equation 2.1.

$$\begin{aligned}\mathbf{V}_{abc s} &= \mathbf{R}_s \mathbf{i}_{abc s} + p \lambda_{abc s} \\ \mathbf{V}_{abc r} &= \mathbf{R}_r \mathbf{i}_{abc r} + p \lambda_{abc r}\end{aligned}\quad (2.1)$$

For a magnetically linear system, the flux linkages can be expressed as

$$\begin{bmatrix} \lambda_{abc s} \\ \lambda_{abc r} \end{bmatrix} = \begin{bmatrix} \mathbf{L}_s & \mathbf{L}_{sr} \\ (\mathbf{L}_{sr})^T & \mathbf{L}_r \end{bmatrix} \begin{bmatrix} \mathbf{i}_{abc s} \\ \mathbf{i}_{abc r} \end{bmatrix}\quad (2.2)$$

The resistance and inductance matrices that appear in the equations have dimensions of 3x3. However, in symmetrical machines, the resistance and inductance matrices related to the stator and rotor leakage inductances are reduced to unit matrices characterised by only two resistive parameters and only two leakage parameters.

$$\mathbf{R}_{abc s}^s = R_s \begin{vmatrix} 1 & 0 & 0 \\ 0 & 1 & 0 \\ 0 & 0 & 1 \end{vmatrix} \quad \mathbf{R}_{abc r}^r = R_r \begin{vmatrix} 1 & 0 & 0 \\ 0 & 1 & 0 \\ 0 & 0 & 1 \end{vmatrix}\quad (2.3)$$

$$\mathbf{L}_l^s = L_{ls} \begin{vmatrix} 1 & 0 & 0 \\ 0 & 1 & 0 \\ 0 & 0 & 1 \end{vmatrix} \quad \mathbf{L}_l^r = L_{lr} \begin{vmatrix} 1 & 0 & 0 \\ 0 & 1 & 0 \\ 0 & 0 & 1 \end{vmatrix}\quad (2.4)$$

Neglecting mutual leakage between the stator windings, and also between the rotor windings, the winding inductances for the Induction Machine may be expressed as:

$$\mathbf{L}_s = \begin{bmatrix} L_{ls} + L_{ms} & -\frac{1}{2}L_{ms} & -\frac{1}{2}L_{ms} \\ -\frac{1}{2}L_{ms} & L_{ls} + L_{ms} & -\frac{1}{2}L_{ms} \\ -\frac{1}{2}L_{ms} & -\frac{1}{2}L_{ms} & L_{ls} + L_{ms} \end{bmatrix}\quad (2.5)$$

$$\mathbf{L}_r = \begin{bmatrix} L_{lr} + L_{mr} & -\frac{1}{2}L_{mr} & -\frac{1}{2}L_{mr} \\ -\frac{1}{2}L_{mr} & L_{lr} + L_{mr} & -\frac{1}{2}L_{mr} \\ -\frac{1}{2}L_{mr} & -\frac{1}{2}L_{mr} & L_{lr} + L_{mr} \end{bmatrix}\quad (2.6)$$

$$\mathbf{L}_{sr} = L_{sr} \begin{bmatrix} \cos \theta_r & \cos \left(\theta_r + \frac{2\pi}{3} \right) & \cos \left(\theta_r - \frac{2\pi}{3} \right) \\ \cos \left(\theta_r - \frac{2\pi}{3} \right) & \cos \theta_r & \cos \left(\theta_r + \frac{2\pi}{3} \right) \\ \cos \left(\theta_r + \frac{2\pi}{3} \right) & \cos \left(\theta_r - \frac{2\pi}{3} \right) & \cos \theta_r \end{bmatrix}\quad (2.7)$$

Where:

- L_{ls} and L_{ms} are the leakage and the magnetizing inductances of the stator windings,
- L_{lr} and L_{mr} are the leakage and the magnetizing inductances of the rotor windings,
- L_{sr} is the amplitude of the mutual inductance between stator and rotor windings. It is affected by the phase shift between stator and rotor windings, varying with rotor position.
- θ_R is the rotor position.

It is convenient to refer all rotor variables to the stator windings using the following turns ratios [7]:

$$\mathbf{i}'_{abc} = \frac{N_r}{N_s} \mathbf{i}_{abc} \quad (2.8)$$

$$\mathbf{v}'_{abc} = \frac{N_s}{N_r} \mathbf{v}_{abc} \quad (2.9)$$

$$\lambda'_{abc} = \frac{N_s}{N_r} \lambda_{abc} \quad (2.10)$$

Similarly, it is possible to refer to the stator windings the magnetizing and mutual inductances associated with the same magnetic flux path.

$$L_{ms} = \frac{N_s}{N_r} L_{sr} \quad (2.11)$$

It is possible to define the mutual inductance between stator and rotor windings as described in Equation 2.12:

$$\mathbf{L}'_{sr} = \frac{N_s}{N_r} \mathbf{L}_{sr} = L_{ms} \begin{bmatrix} \cos \theta_r & \cos \left(\theta_r + \frac{2\pi}{3} \right) & \cos \left(\theta_r - \frac{2\pi}{3} \right) \\ \cos \left(\theta_r + \frac{2\pi}{3} \right) & \cos \left(\theta_r - \frac{2\pi}{3} \right) & \cos \theta_r \end{bmatrix} \quad (2.12)$$

Rotor winding inductance should be also referred to stator quantities using the transformation ratio $\left(\frac{N_s}{N_r}\right)^2$:

$$\mathbf{L}'_r = \left(\frac{N_s}{N_r}\right)^2 \mathbf{L}_r \quad (2.13)$$

Magnetizing inductance of rotor and stator windings are related accordingly with Equation 2.14.

$$L_{mr} = \left(\frac{N_r}{N_s}\right)^2 L_{ms} \quad (2.14)$$

Accordingly with Equation 2.13, using equations 2.14 and 2.2, the rotor winding inductance referred to stator quantities L'_r is computed:

$$\mathbf{L}'_r = \begin{bmatrix} L'_{lr} + L_{ms} & -\frac{1}{2}L_{ms} & -\frac{1}{2}L_{ms} \\ -\frac{1}{2}L_{ms} & L'_{lr} + L_{ms} & -\frac{1}{2}L_{ms} \\ -\frac{1}{2}L_{ms} & -\frac{1}{2}L_{ms} & L'_{lr} + L_{ms} \end{bmatrix} \quad (2.15)$$

Where rotor windings leakage inductance referred to stator is computed using the same transformation ratio $(\frac{N_s}{N_r})^2$, as in 2.13 and in 2.14:

$$L'_{lr} = \left(\frac{N_s}{N_r}\right)^2 L_{lr} \quad (2.16)$$

Since all the requested quantities have been defined, it is possible to rewrite the electrical and magnetic equations. As shown in 2.17 and 2.18, all the rotor quantities are referred to stator windings:

$$\begin{bmatrix} \lambda_{abc} \\ \lambda'_{abcr} \end{bmatrix} = \begin{bmatrix} \mathbf{L}_s & \mathbf{L}'_{sr} \\ (\mathbf{L}'_{sr})^T & \mathbf{L}'_r \end{bmatrix} \begin{bmatrix} \mathbf{i}_{abc} \\ \mathbf{i}'_{abcr} \end{bmatrix} \quad (2.17)$$

$$\begin{bmatrix} \mathbf{v}_{abc} \\ \mathbf{v}'_{abcr} \end{bmatrix} = \begin{bmatrix} \mathbf{R}_s + p\mathbf{L}_s & p\mathbf{L}'_{sr} \\ p(\mathbf{L}'_{sr})^T & \mathbf{R}'_r + p\mathbf{L}'_r \end{bmatrix} \begin{bmatrix} \mathbf{i}_{abc} \\ \mathbf{i}'_{abcr} \end{bmatrix} \quad (2.18)$$

Where R'_r is the rotor winding resistance 2.19 referred to stator windings, computed using the transformation ratio $(\frac{N_s}{N_r})^2$, already used for rotor inductances.

$$\mathbf{R}'_r = \left(\frac{N_s}{N_r}\right)^2 \mathbf{R}_r \quad (2.19)$$

Based on what we have seen so far, the mathematical model of the machine is therefore made up of a system of six differential equations of the first order, associated with a system of six ordinary equations linear. In addition to the instantaneous position $\theta(t)$ of the rotor, it is characterised by the following five parameters:

$$R_s, R'_r, L_{ls}, L'_{lr}, L_m \quad (2.20)$$

where L_m is the mutual inductance between stator and rotor windings:

$$L_m = \frac{3}{2}L_{ms} \quad (2.21)$$

2.3 Equations of Transformation

In order to simplify the electrical and magnetic equations that describe the dynamic behaviour of the machine, it can be useful to introduce the idea of equivalent bi-phase machine. Its windings are shifted of 90 electrical degrees and, for this reason, a lot of mutual coupling coefficients become equal to zero and the number of equations is reduced from six to four.

The most convenient choice for studying transient behaviour of an induction machine is to refer the machine variable to a d,q rotating reference frame, where q-axis lags the d-axis by 90° .

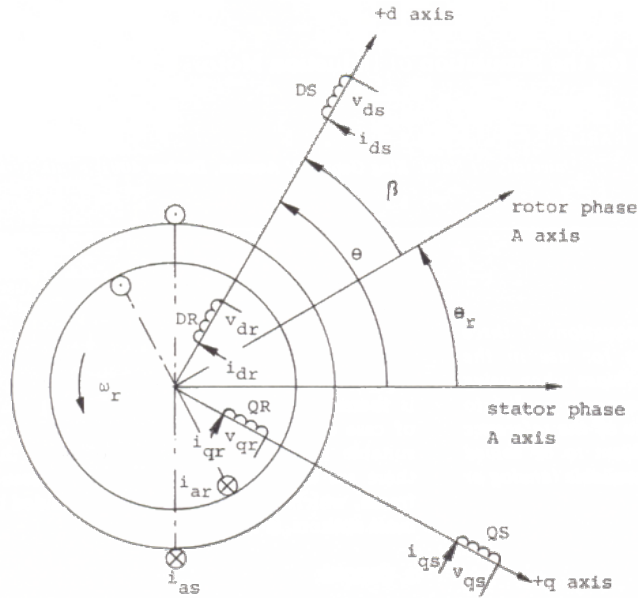


Figure 2.2: d,q axes in a three-phase induction motor

In order to predict the mechanical and the electrical behaviour of the original Induction machine correctly, the ABC variables should be transformed into d,q variables [9]. This process of transformation will be affected by the choice of the speed of the rotation of d,q - frame, because each reference frame has its own transformation. If $\omega = p\theta$ is the arbitrary speed of d,q frame the transformation from ABC phase variables $[F_{ABC}]$ to d,q variables $[F_{dq0}]$ is performed by Park's transformation:

$$[F_{0dq}] = [P_\theta] [F_{ABC}] \quad (2.22)$$

Where

$$[P_\theta] = 2/3 \begin{bmatrix} 1/2 & 1/2 & 1/2 \\ \cos \theta & \cos(\theta - \frac{2\pi}{3}) & \cos(\theta + \frac{2\pi}{3}) \\ \sin \theta & \sin(\theta - \frac{2\pi}{3}) & \sin(\theta + \frac{2\pi}{3}) \end{bmatrix} \quad (2.23)$$

The voltage equations for d,q coils are define as:

$$\begin{aligned} v_{ds} &= R_s i_{ds} + p\psi_{ds} + \psi_{qs} p\theta \\ v_{qs} &= R_s i_{qs} + p\psi_{qs} - \psi_{ds} p\theta \\ v_{dr} &= R_r i_{dr} + p\psi_{dr} + \psi_{qr} p\beta \\ v_{qr} &= R_r i_{qr} + p\psi_{qr} - \psi_{dr} p\beta \end{aligned} \quad (2.24)$$

Where:

$$\begin{bmatrix} \psi_{ds} \\ \psi_{dr} \\ \psi_{qs} \\ \psi_{qr} \end{bmatrix} = \begin{bmatrix} L_s & L_m & 0 & 0 \\ L_m & L_r & 0 & 0 \\ 0 & 0 & L_s & L_m \\ 0 & 0 & L_m & L_r \end{bmatrix} \begin{bmatrix} i_{ds} \\ i_{dr} \\ i_{qs} \\ i_{qr} \end{bmatrix} \quad (2.25)$$

and $L_s = L_{ls} + L_m$, $L_r = L_{lr} + L_m$. As shown in the next two sections, for the purposes of this project, the dynamic motor model was developed in two reference frames: rotor and rotor flux reference frame.

Figure 2.3 shows the equivalent circuit of an induction motor in d,q frame. However the reference frame speed can be chosen arbitrary, it is common, for control purposes to set it equal to zero (stationary reference frame), to rotor speed (rotor reference frame) or to synchronous speed (synchronous reference frame).

Note that all rotor quantities are referred to stator windings ($R_r = R'_r$, $L_r = L'_r$ and $L_{lr} = L'_{lr}$). To relieve the notation, it is preferred to remove the superscript.

2.4 Rotor Reference Frame

In this reference frame the d-axis of the reference frame is moving at the same relative speed as the rotor phase A winding (If they are coincident, it should be expected that the behaviour of the d-axis current and phase A current would be identical). Referring to Figure 2.2:

$$\begin{aligned} \omega &= p\theta = \omega_r \\ \beta &= \theta - \theta_r = 0 \\ p\beta &= 0 \end{aligned} \quad (2.26)$$

Substituting Equations 2.26 in 2.24:

$$\begin{aligned} v_{ds} &= R_s i_{ds} + p\psi_{ds} + \omega_r \psi_{qs} \\ v_{qs} &= R_s i_{qs} + p\psi_{qs} - \omega_r \psi_{ds} \\ v_{dr} &= R_r i_{dr} + p\psi_{dr} \\ v_{qr} &= R_r i_{qr} + p\psi_{qr} \end{aligned} \quad (2.27)$$

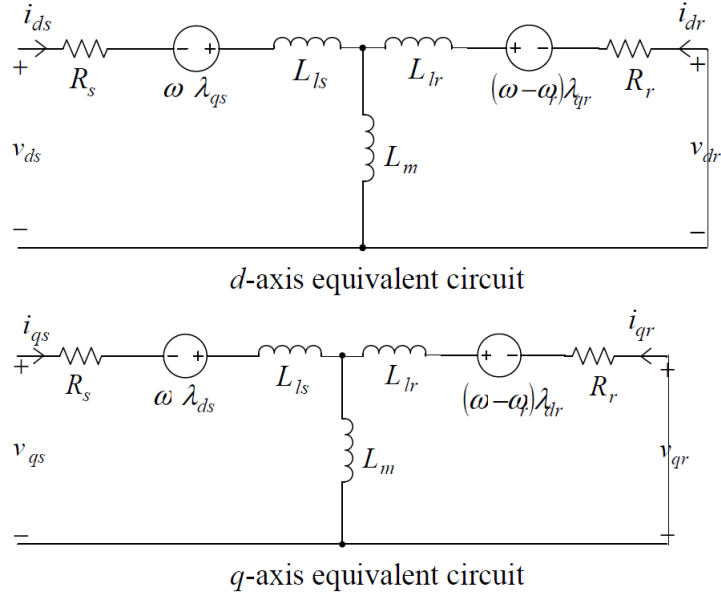


Figure 2.3: dq - Induction Motor Equivalent Circuit

Combining Equation 2.27 with 2.25 and manipulating the results in order to make

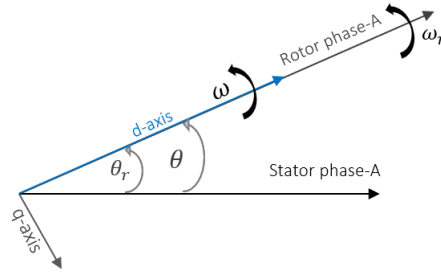


Figure 2.4: Rotor Reference Frame

explicit the equations as a function of stator currents [10], equations 2.28 and 2.29 are obtained. Note that, since the the induction machine has a squirrel-cage rotor $v_{dr} = v_{qr} = 0$.

$$\frac{di_{sd}}{dt} = \frac{v_{sd} - R_s \cdot i_{sd} + \frac{L_s(1-\sigma)}{\tau_R} \cdot i_{rdm} + L_s \cdot \omega_r \cdot i_{sq} + L_s \cdot (1-\sigma) \cdot \omega_r \cdot i_{rqm}}{\sigma \cdot L_s} \quad (2.28)$$

$$\frac{di_{sq}}{dt} = \frac{v_{sq} - R_s \cdot i_{sq} + \frac{L_s(1-\sigma)}{\tau_R} \cdot i_{rqm} - L_s \cdot \omega_r \cdot i_{sd} - L_s \cdot (1-\sigma) \cdot \omega_r \cdot i_{rdm}}{\sigma \cdot L_s} \quad (2.29)$$

where:

- $\sigma = 1 - \frac{L_m}{L_s \cdot L_r}$ is called *dispersion coefficient* and takes into account the total leakage;
- $\tau_R = \frac{L_r}{R_r}$ is the *rotor time constant*.
- $i_{rdm} = \frac{L_m}{L_r} i_{rd}$ and $i_{rqm} = \frac{L_m}{L_r} i_{rq}$ are the modified d,q rotor currents.

Electromagnetic torque has been obtained as follow:

$$T_{em} = p(1 - \sigma) \cdot L_s \cdot (i_{rdm} \cdot i_{sq} - i_{rqm} \cdot i_{sd}) \quad (2.30)$$

IM dynamic model in rotor reference frame was built directly implementing Equations 2.28, 2.29 and 2.30 in Simulink environment (Figure 2.5).

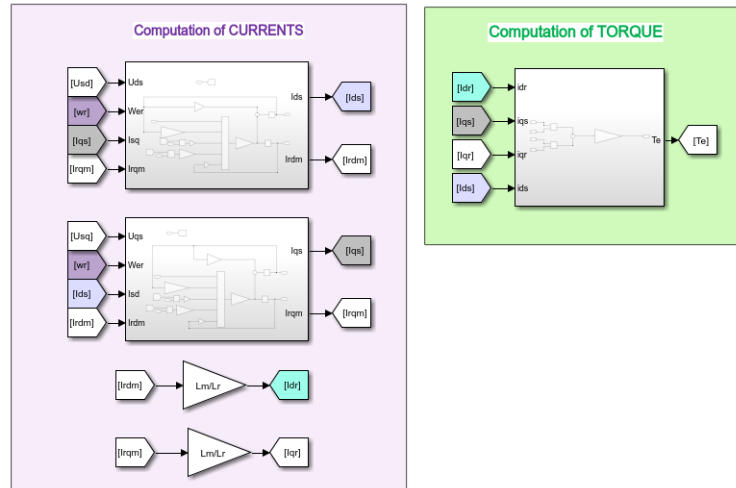


Figure 2.5: IM model in rotor reference frame - Simulink implementation

2.5 Rotor Flux Reference Frame

Rotor flux reference frame is of particular interest because it is widely exploited in Field Oriented control (FOC) of asynchronous motors. Using vector control,

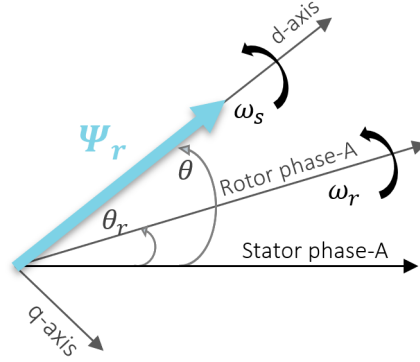


Figure 2.6: Rotor Flux Reference Frame

induction machines can be controlled to give dynamic performance comparable to the separately excited DC motor. There are at least three fluxes, rotor, airgap and stator and three currents, stator, rotor and magnetizing in an induction motor. For high dynamic response, interactions among current, fluxes, and speed must be taken into account in determining appropriate control strategies. By fixing the d,q rotating frame with rotor flux vector, independent control of motor flux and torque can be achieved. The the d-q reference frame is rotating at the same rotor flux vector angular speed ω_s (Figure 2.6). Referring to Figure 2.2:

$$\begin{aligned}\omega &= p\theta = \omega_s \\ \beta &= \theta - \theta_r = \omega_s t - \theta_r \\ p\beta &= \omega_s - \omega_r\end{aligned}\quad (2.31)$$

Substituting Equations 2.31 in 2.24:

$$\begin{aligned}v_{ds} &= R_s i_{ds} + p\psi_{ds} + \omega_s \psi_{qs} \\ v_{qs} &= R_s i_{qs} + p\psi_{qs} - \omega_s \psi_{ds} \\ v_{dr} &= R_r i_{dr} + p\psi_{dr} + (\omega_s - \omega_r) \psi_{qr} \\ v_{qr} &= R_r i_{qr} + p\psi_{qr} - (\omega_s - \omega_r) \psi_{dr}\end{aligned}\quad (2.32)$$

To obtain the equations finally implemented in the system-level model, it is necessary to manipulate Equations 2.32. Using the assumption that d-axis is aligned with rotor flux vector:

$$\begin{aligned}\psi_{rq} &= 0 \\ \psi_{rd} &= \psi_r\end{aligned}\quad (2.33)$$

Using the first equation in 2.33 and studying q-axis rotor flux:

$$\begin{aligned} \frac{d\psi_{rq}}{dt} &= 0 \\ \psi_{rq} &= L_r i_{rq} + L_m i_{sq} = 0 \end{aligned} \quad (2.34)$$

The magnetizing current i_{mr} , responsible for the magnetizing flux generation, is equal to the torque producing component of the stator current i_{sq} at steady state condition. It is related to d-axis rotor flux as follows:

$$\psi_{rd} = L_m i_{mr} \quad (2.35)$$

The magnetizing current dependency on the d component of stator current is obtained as:

$$\begin{aligned} \frac{d\psi_{rd}}{dt} + R_r i_{rd} &= 0 \\ \tau_r \frac{di_{mr}}{dt} + i_{mr} &= i_{sd} \\ i_{mr} &= \frac{i_{sd}}{(1+s\tau_r)} \end{aligned} \quad (2.36)$$

where τ_R is the rotor time constant, presented in Section 2.4.

Also in this case, it is possible to re-write the voltage equations as functions of stator currents. Stator currents and electromagnetic torque are presented in 2.37, 2.38 and 2.39, as they were implemented for building the IM motor model in Simulink environment (Figure 2.7).

$$\frac{di_{sd}}{dt} = \frac{v_{sd} - i_{sd} \cdot R_s + i_{rd} \sqrt{\frac{L_s(1-\sigma)}{\tau_R}}}{L_s \cdot \sigma} + i_{sq} \cdot \omega_s \quad (2.37)$$

$$\frac{di_{sq}}{dt} = \frac{v_{sq} - i_{sq} \cdot R_s - \omega_s (i_{rd} \sqrt{L_s(1-\sigma)\tau_R} + i_{sd} \cdot L_s)}{L_s \cdot \sigma} \quad (2.38)$$

$$T_{em} = p(i_{rd} \cdot i_{sq} - i_{rq} \cdot i_{sd}) \sqrt{L_s(1-\sigma)\tau_R} \quad (2.39)$$

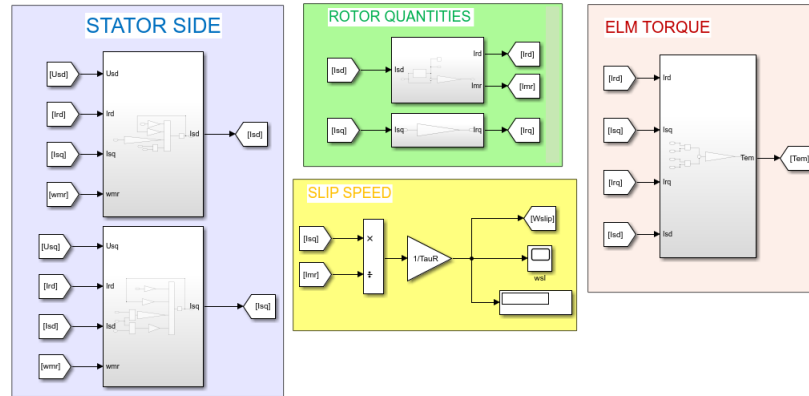


Figure 2.7: IM model in rotor flux reference frame - Simulink implementation

2.6 Simulink Implementation

The previous sections explain how to derive a dynamic model of an Induction machine in two different d,q-reference frames. These equations were implemented in Simulink environment and permit to study the response of the motor to a transient, as well as the coupling with different drive. The choice to develop the model in two frames was done in order to make free the future user to easily implement different kind of control algorithms.

As shown in Figure 2.8 Simulink model is mainly developed in four parts:

- PART 1: Definition of the operating point.
The user can decide to specify the operating point imposing Rotor Speed or Load Torque. All the parameters related to the design choices are imported in Simulink environment from the design sheet produced by PC-IMD in SPEED, as well as the information related to the operating point (ω_R , T_L).
- PART 2: Choice of the drive.
Here, the way are three-phase voltages are imposed is defined. At this stage of the project it is possible to choose between:
 - Sinusoidal Voltage source;
 - Current controller;
 - Scalar Control.

Because this project is not focused in control, an ideal sinusoidal voltage source was mainly used. However, this section was implemented to permits the future user to define drives, since, would be interesting to study how different drives impact on noise and vibrations.

- PART 3: Choice of the d,q model.
The user can choose between Rotor and Rotor Flux Reference frame. Moreover, for each reference, there are two models: one with constant magnetizing inductance and the other with varying L_m , as discussed in next section.
- PART 4: Post-processing
In this part, even with some approximation, a first approximation of the losses is computed (in the equivalent circuit, Iron resistance is neglected). Moreover, the rms values of stator, rotor and magnetizing current are computed, as well as the phase shift between stator and rotor phasors.

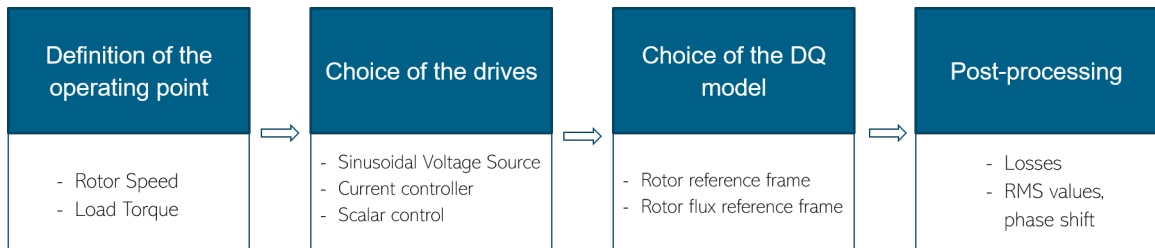


Figure 2.8: System-level model

2.7 Inclusion of the saturating effect of the magnetizing inductance

The models discussed throughout the previous pages consider constant equivalent circuit parameters (i.e. resistances and inductances). However, they vary according the operating point at which the induction machine is working [11].

This section aims to explain how the effect of saturation impacts on the value of the magnetizing inductance. Stator and Rotor leakage inductance are considered constant: modelling them variation depending on the operating point could be a further development.

The system-level model in Simulink was slightly modified to include this aspect. As shown in Figure 2.9, the value of magnetizing inductance L_m will vary accordingly the magnetizing current. Estimated I_m , the correspondent value of L_m is selected and the induction motor model receives his as input.

Using SPEED's PC-FEA it is possible to perform a no-load simulation feeding the stator within a specified range of current. The results of that simulation are shows in the left side of Figure 2.10. It is so possible to extract a curve magnetizing flux

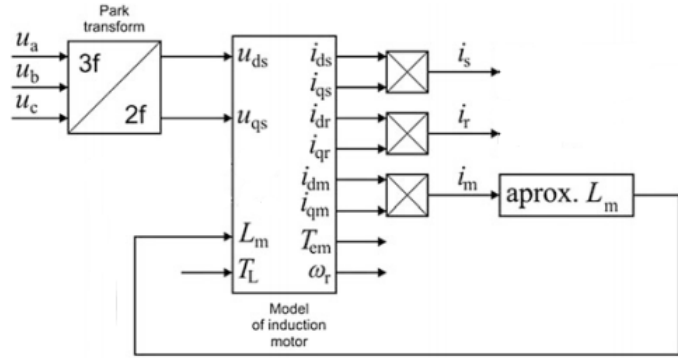


Figure 2.9: Modified Induction Motor model

versus magnetizing current, for a specified motor design. The value of apparent and differential inductances are shown in the right side of Figure 2.10.

At this stage, the magnetizing inductance L_m is supposed to be equal to the apparent inductance, computed as $L_m = \frac{\Psi_m}{I_m}$. L_m and relative values of I_m are stored into a Look Up Table, that is used in Simulink model in order to take into account the effect of saturation.

In figure 2.10 three operating point are underlined: one in the linear region, one in the knee and the other in saturated part of the magnetizing curve. The variation of L_m affects the behaviour of the machine during the transient.

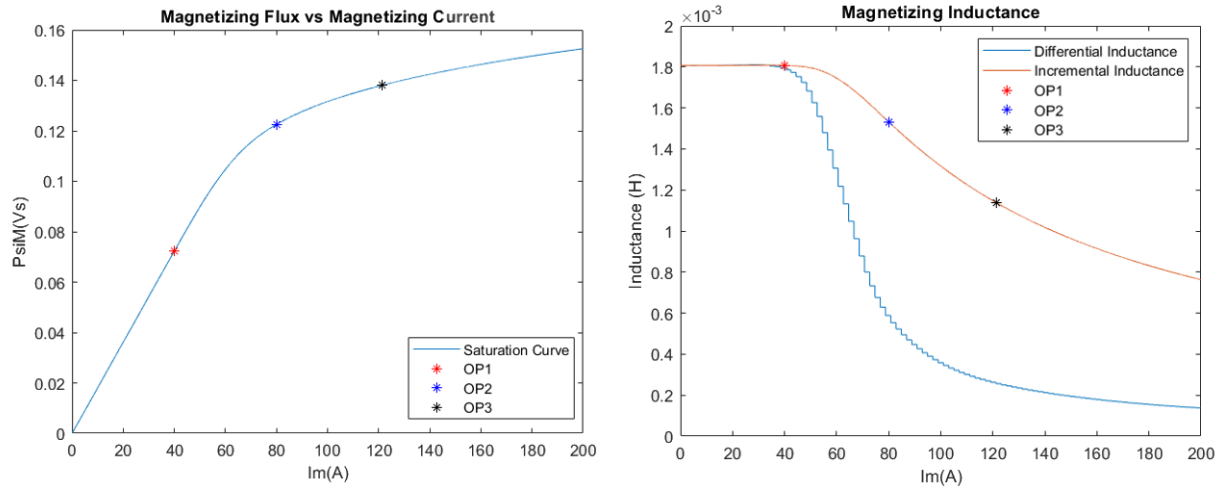


Figure 2.10: Magnetizing Effect of Saturation Inductance

2.8 Coupling Simulink Model with FEA

The model was mainly validated by comparing the results with those of the commercial software Amesim, whose blocks (EMDSCIM01 and EMDSCIM02) use the same equations. For different values of the equivalent circuit parameters (i.e. resistances and inductances) and operating points, the machine variables were compared and their identities were demonstrated.

Another interesting test, for IM system-level model validation and coupling with SPEED design software, was the comparison between stator flux linkages, calculated with the dynamic model and the results of the On-load test performed with PC-FEA (Section 1.4.2).

In the On Load test, the operating point is specified (peak value of the stator and rotor current, phase-shift between phases), together with the initial position of the rotor axis and the number of steps that the rotor has to perform to make a complete rotation (In this test 45 steps). The test was conducted for the Kyburz eRod motor design (Section 1.4.3) at rated power. The results of the comparison is shown in Figure 2.11.

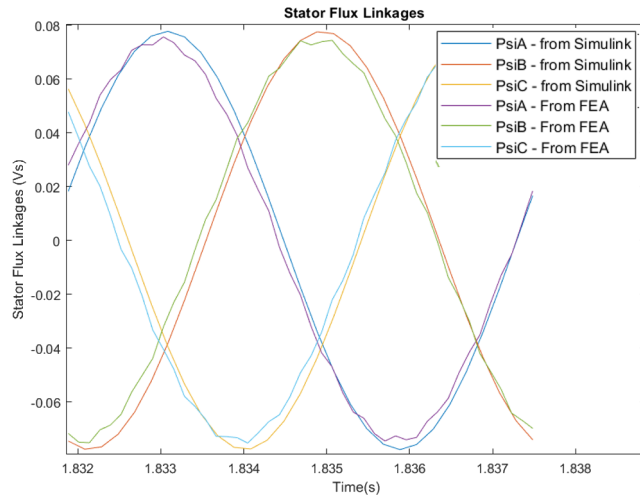


Figure 2.11: Flux linkages

Chapter 3

Stator Magnetomotive Force

In this chapter the magnetomotive force due to the stator of a polyphase induction machine will be discussed . The poliphase winding, usually three phase, is located in stator core slots. It has been assumed that the stator is fed with a balanced system of sinusoidal currents. Stator currents (amplitude and phase) and stator winding functions are needed in order to define the stator magnetomotive Force [12], as shown in Equation 3.1:

$$A_S(t, \alpha_S) = \sum_{m=1}^3 I_S^m(t) \cdot N_S^m(\alpha_S) \quad (3.1)$$

Where:

- A_S stator magnetomotive force;
- t time;
- α_S air-gap position
- I_S^m m-phase stator current (in a three phase system m=3);
- N_S m-phase stator winding function.

Accordingly to the convention used in this work, α_S should be intended as an axis which extends over the entire length of the air gap, which does not rotate, being fixed to the stator. If the stator has N slot, $\alpha_S = 0$ in the middle of the Nth-stator slot and it is defined between 0 and 2π .

3.1 Characterisation of a winding

Stator windings are described coherently with the convention used by PC-IMD Winding Editor. For each phase, a coil list table shows the Go and Return slot

numbers (Figure 3.1). Go and Return conductors have different colours to highlight the polarity (North/South) of the winding.

Other specification for winding definitions are:

- Winding Type: Concentric with equal turns/coil, Concentric with sine-distributed turns/coil, Integral-slot lap winding, Fractional-slot winding, Customised.
- TC: Number of turns per coil.
- CPP: Number of coils per pole-group.
- Span of the widest coil in any pole-group.
- Offset in slot-pitches between phase winding starts.

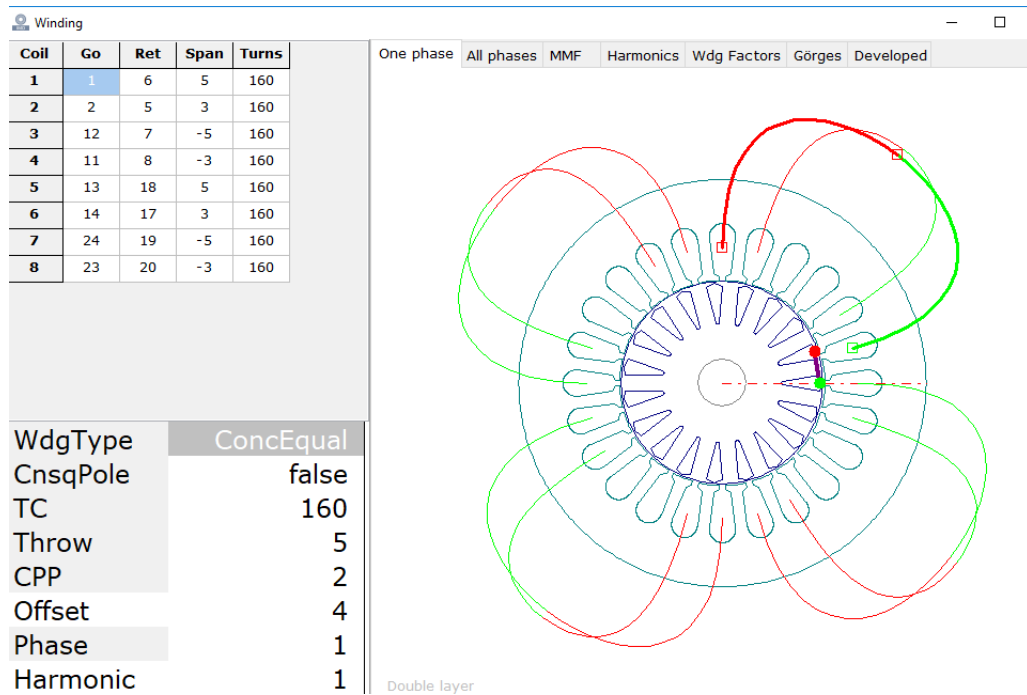


Figure 3.1: PC-IMD Winding Editor

PC-IMD allows to export easily in a .wdg file the specifications related to a winding layout (Figure 3.2). For a symmetrical Induction Machine these information are sufficient to define the winding functions for all stator phases, as described in Section 3.2.

```

Custom winding table
54 1 IMD
24 slots
4 poles
1 Balwdg=TRUE
4 Offset
2 Connex
8 coils/phase
Ph   Go   Ret   Trn
1    1    6    160
1    2    5    160
1   12    7    160
1   11    8    160
1   13   18    160
1   14   17    160
1   24   19    160
1   23   20    160

```

Figure 3.2: Winding Editor - Export winding

3.2 Winding functions definition

This section shows how to compute the winding functions for the three phases of the stator. Winding function is defined according to Equation 3.2:

$$N_A(\alpha_S) = \begin{cases} \pm N_{\text{turns}}, & \alpha_1 \leq \alpha_S \leq \alpha_2 \\ 0 & \text{rest of } \alpha_S \end{cases} \quad (3.2)$$

Where N_{turns} is the number of turns per coil (in a parallel path) and $\tau = \alpha_2 - \alpha_1 = |\text{Ret} - \text{Go}|$ is the coil pitch. To define the sign of the function ($\pm N_{\text{turns}}$), it is necessary to investigate the winding data. As shown in Figure 3.1, each coil is characterised with a Go and Ret value. This means that the winding is built going from slot Go to slot Ret. For each coil of the winding is used the sign:

$$\begin{aligned} &+ \text{ if } \text{Go} < \text{Ret} \\ &- \text{ if } \text{Go} > \text{Ret} \end{aligned} \quad (3.3)$$

And the air-gap positions α_1 and α_2 are defined accordingly to Equations 3.4 and 3.5:

$$\alpha_1 = \begin{cases} \text{Go} \cdot \frac{2\pi}{N_{\text{cages}}}, & \text{if } \text{Go} < \text{Ret} \\ \text{Ret} \cdot \frac{2\pi}{N_{\text{cages}}}, & \text{if } \text{Go} > \text{Ret} \end{cases} \quad (3.4)$$

$$\alpha_2 = \begin{cases} \text{Ret} \cdot \frac{2\pi}{N_{\text{cages}}}, & \text{if } G_O < \text{Ret} \\ G_O \cdot \frac{2\pi}{N_{\text{cages}}}, & \text{if } G_O > \text{Ret} \end{cases} \quad (3.5)$$

Figure 3.3 shows the winding function of Phase A, for the layout presented in Figure 3.1. A 2 pole-pairs induction machine, with 24 slots and $N_{\text{turns}} = 160$ is considered.

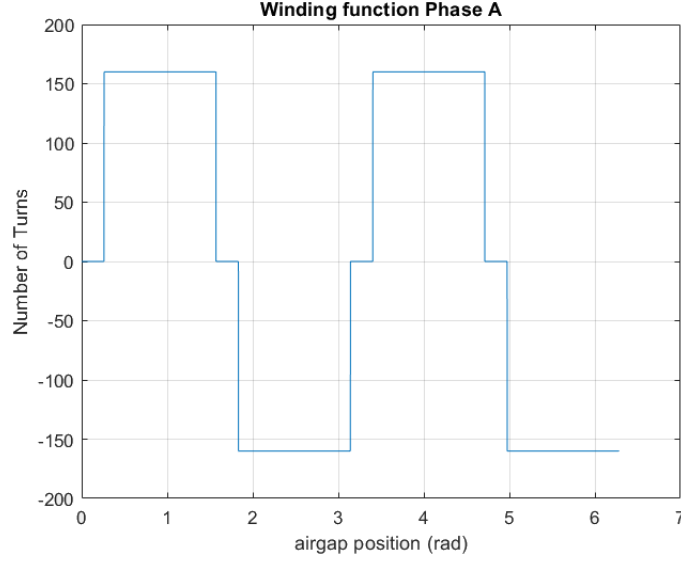


Figure 3.3: Winding Function - Phase A

Concerning Phase B and C, it will be necessary to shift the previous winding function of an Offset defined as the number of slot-pitches between the start of phase 1 and the start of phase 2 (Figure 3.4). Normally, For three-phase motors, the shift angle between two different phases is equal to $120^\circ/\text{pole pairs}$. Expressing this shift in terms of number of slots: $\text{Offset} = \frac{2}{3} \times \frac{\text{Slots}}{\text{Poles}}$.

3.3 Analytical computation of Radial Magnetic Induction in MATLAB

For the purposes of the work, only the radial component of the magnetic flux density B is of interest. It is analytically computed in MATLAB script according to [12]:

$$B_{r,\text{airgap}}(t, \alpha_s) = \Lambda_{\text{air}}(t, \alpha_s) \cdot (A_s(t, \alpha_s) + A_r(t, \alpha_s)) \quad (3.6)$$

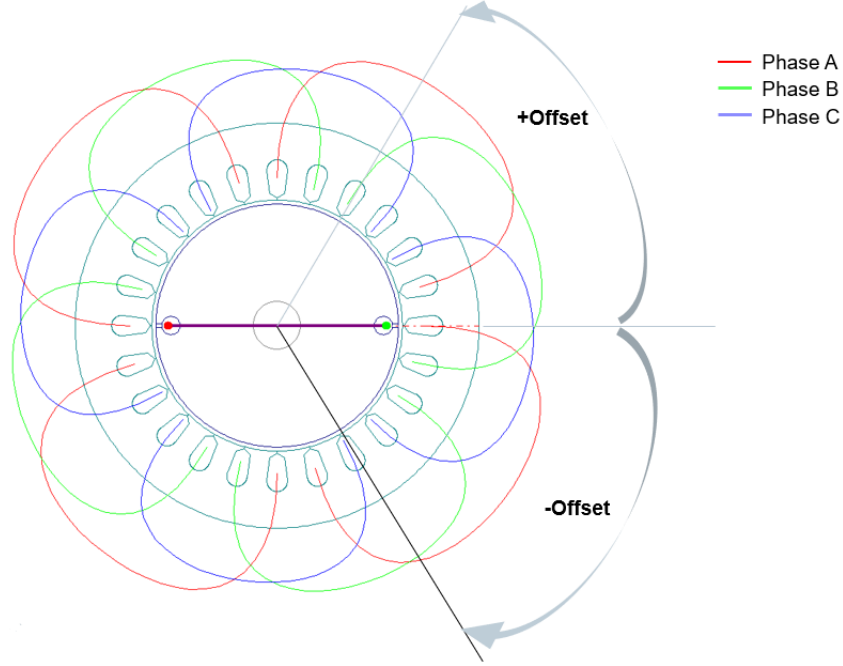


Figure 3.4: Winding Layout - All Phases

Where $\Lambda_{air}(t, \alpha_s)$ is the permeance of the air-gap. At this stage, it is considered as a constant value: $\Lambda_{air} = \frac{\mu_0}{\delta_{id}}$ (where $\mu_0 = 4\pi 10^{-7} \frac{H}{m}$ is the air permeability, and $\delta_{id} = 1mm$ is ideal air-gap thickness - neglecting the presence of stator and rotor slots and iron saturation). Since no current flows into the rotor bars, $A_r(t, \alpha_s) = 0$ and $B_{r,airgap}(t, \alpha_s)$ is only due to the stator

Stator magnetomotive force is computed accordingly with Equation 3.1:

$$A_S(t, \alpha_S) = \sum_{m=1}^3 I_S^m(t) N_S^m(\alpha_S) = I_A(t) N_A(\alpha_S) + I_B(t) N_B(\alpha_S) + I_C(t) N_C(\alpha_S) \quad (3.7)$$

Figure 3.5 shows the stator magnetomotive forces due to each phase and their sum for Kyburtz eRod (Section 1.4.3), at rated power operating point.

3.4 Testing the Stator MMF

The analytical model of the stator magnetomotive force has been validated by comparison with PC-FEA results. PC-FEA is a fast, scriptable fine-element solver

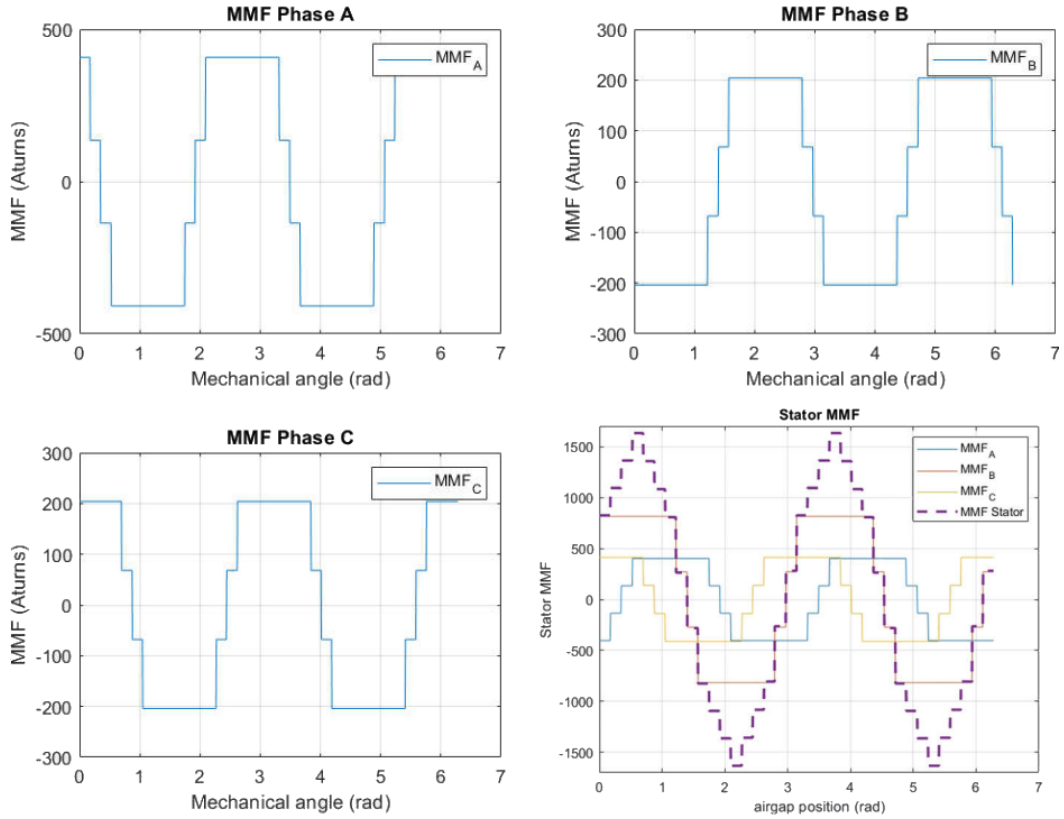


Figure 3.5: Stator Magnetomotive Force

for 2D magnetostatic and thermal calculations (Section 1.4.2). Performing Single Load Point Analysis, the solver calculates the distribution of air-gap flux density at a particular rotor position and a particular load.

Because only the radial component is of interest for this project, only B_R is compared with the analytical results. In order to isolate the contribution to the radial magnetic flux density due to stator windings only, some modification in the induction motor design and in the PC-FEA interface GoFER (Section 1.4.2) should be done. Indeed, at this stage, the permeability of stator and rotor iron lamination is assumed infinite, the air-gap thickness constant and the rotor to be a disk with no bars or windings. In the list below, the assumptions and the amplification performed are discussed more in details:

- Assumption 1: " The effect of slot opening is negligible and the air-gap depth can be considered to be constant":

Stator slot openings are set to be equal the minimum allowed by the design software. Rotor slots are closed.

- Assumption 2: *"The rotor is a disk, without bars or windings"*:

The rotor, for this test, has only two bars (since two is the minimum number allowed by PC-IMD). Moreover, in the FE user interface (GOFER) zero current flowing in the rotor bars was imposed.

- Assumption 3: *"Iron permeability is infinite"*:

The operating points considered in this test are referred to relatively low stator current values. In this way, the hypothesis of working in a linear zone of B-H curve is valid and the magnetic induction calculated in this way won't be interest on saturation effects.

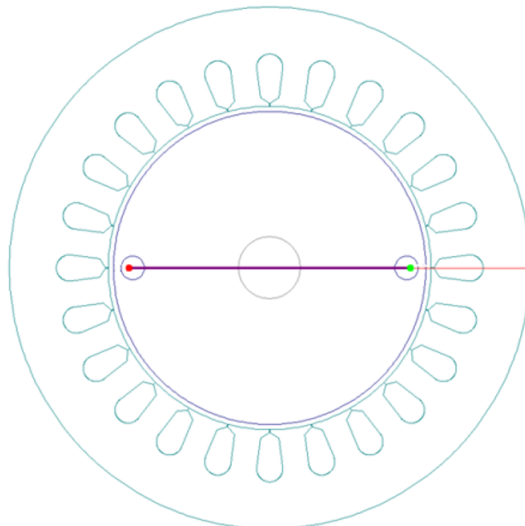


Figure 3.6: Simplified Geometry for testing stator MMF

3.4.1 Single Load Point Finite Element Analysis

The Single load point GoFER 1.4.2 produces a finite-element solution at a fixed rotor angle [6]. It returns the air-gap flux-density distribution and the torque calculated by Maxwell stress.

For polyphase motors operating under balanced conditions, it is sufficient to specify the current in one phase of the stator and one phase of the rotor. For example, in

a three-phase motor, if stator current amplitude (peak value) is equal \hat{I} and the electrical angle is $\theta = \omega \cdot t$:

$$\begin{aligned} i_A(t) &= \hat{I} \cos(\omega t) \\ i_B(t) &= \hat{I} \cos\left(\omega t - \frac{2\pi}{3}\right) \\ i_C(t) &= \hat{I} \cos\left(\omega t + \frac{2\pi}{3}\right) \end{aligned} \quad (3.8)$$

Similar relations hold for the rotor currents.

Figures 3.7 and 3.8 shows the results of a PC-FEA simulation for the simplified design shown in Figure 3.6, with a $\hat{I}_S = 10A$, $\theta = \omega \cdot t = 0$, $\hat{I}_R = 0A$ and rotor reference axis is coincident with $\alpha_S = 0$ (i.e. in the middle of the Nth slot).

Figure 3.7 shows the distribution of the vector potential and of the magnetic flux density for the specified operating point.

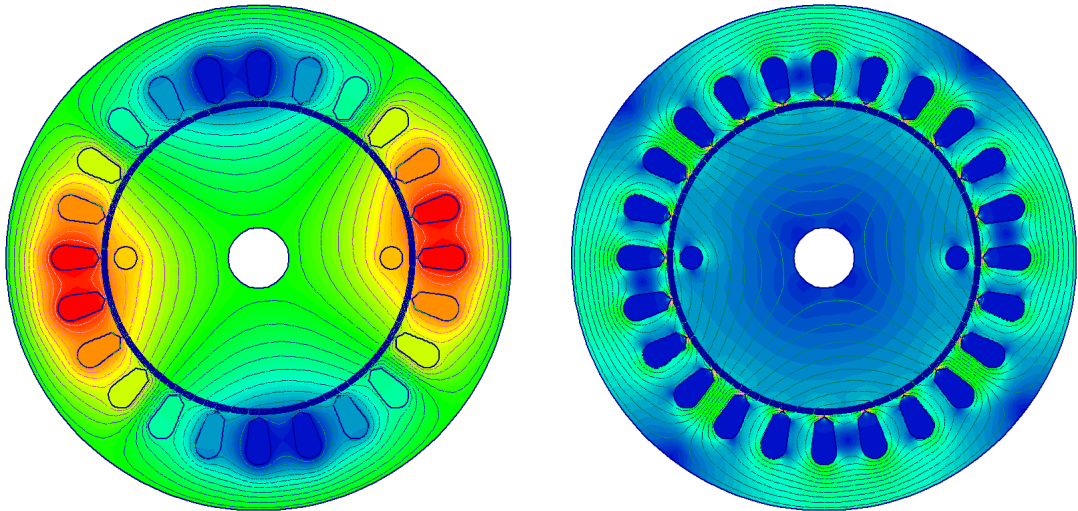


Figure 3.7: FEA results: Zone paint: Vector Potential and Magnetic flux density, Equipotential lines: Vector Potential

In Figure 3.8 both the radial (in red) and the tangential (in green) component of the magnetic flux density are shown. For what concerns this project, only the radial component of the magnetic induction is of interest.

Figure 3.9 compares the Magnetic Induction obtained analytically with PC-FEA results, using the same inputs in both the calculations.

The same process is repeated for different electrical positions (Figure ??) and for different winding layout.

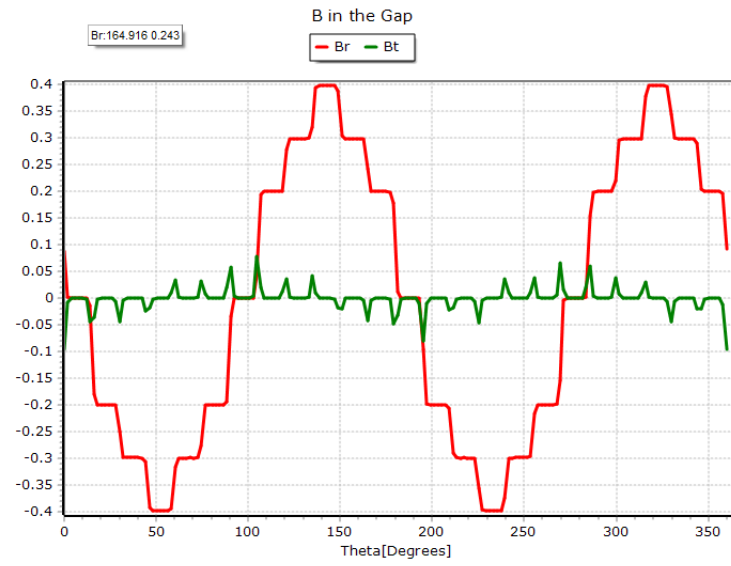


Figure 3.8: Radial and Tangential Magnetic Induction in the air-gap

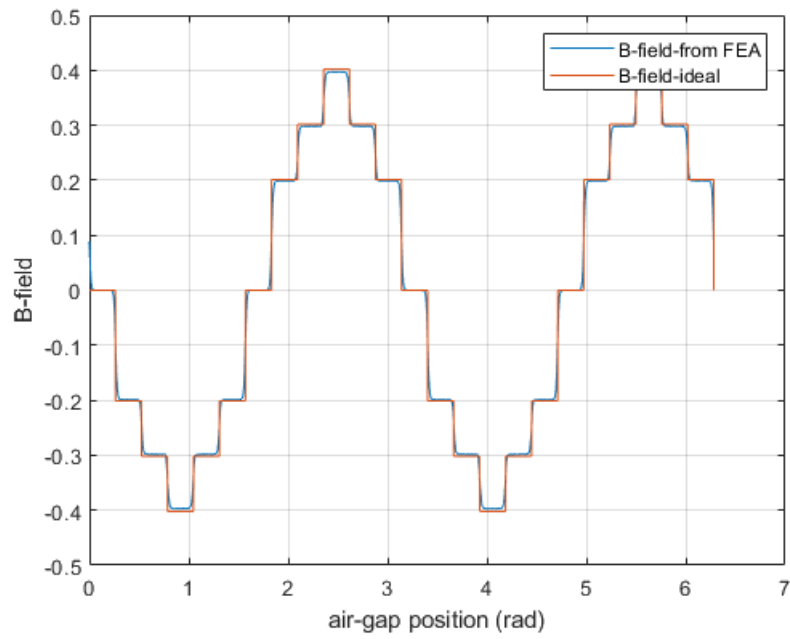
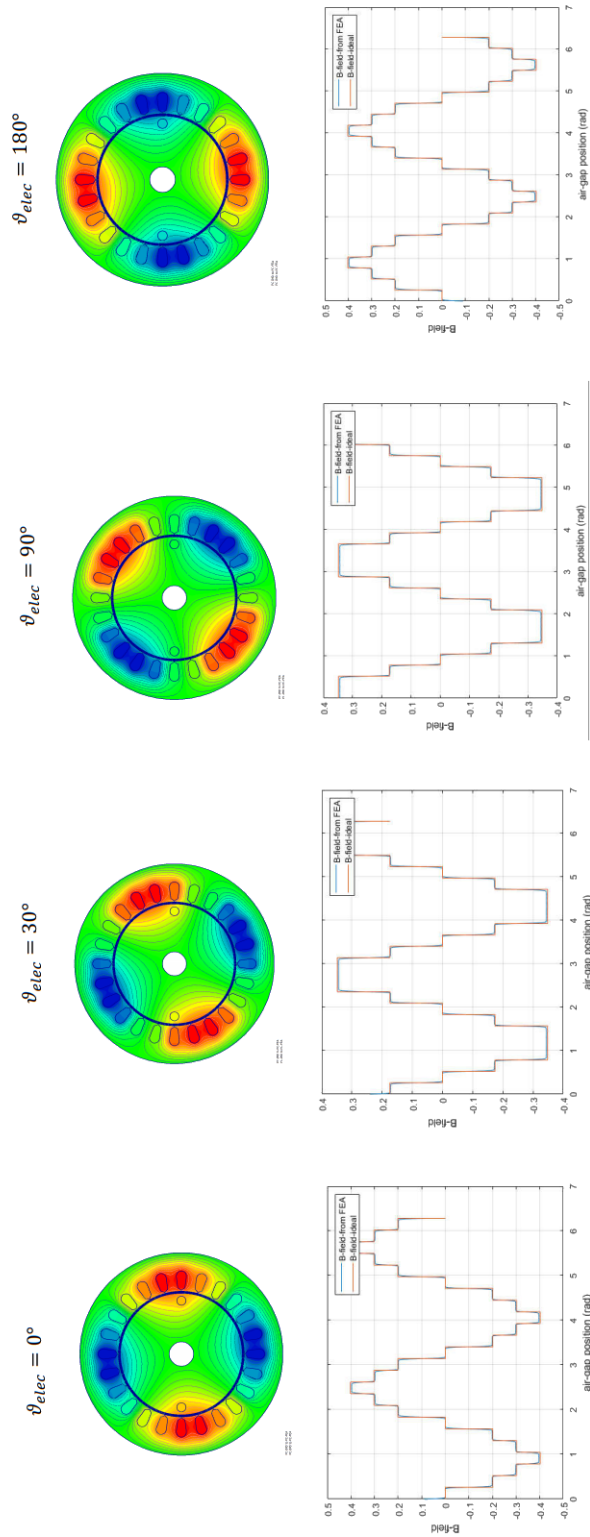


Figure 3.9: Comparison between FEA and analytical results



39
Figure 3.10: Comparison between FEA and analytical results: different electrical positions

Chapter 4

Rotor Magnetomotive Force

The rotor magnetomotive force was computed with a similar approach compared to the stator MMF. The squirrel cage rotor is considered as a polyphase system, where the number of phases is equal to the number of bars. For that reason, the expression of rotor magnetomotive force [12] will appear as shown in Equation 4.1:

$$A_R(t, \alpha) = \sum_{k=0}^{Q_R-1} I_R^k(t) \cdot N_R^k(\alpha) \quad (4.1)$$

Where:

- A_R rotor magnetomotive force;
- t time;
- α_S air-gap position
- I_S^m m-phase stator current (in a three phase system $m=3$);
- N_S m-phase stator winding function.

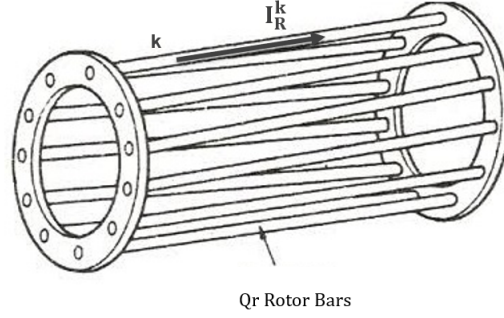
4.1 Current distribution in rotor bars

On the rotor side, the magnitude of the rotor current vector is split up into the current per rotor bar (Figure 4.1), with the assistance of a sinusoidal function:

$$I_R^k(t) = |\vec{i}_R(t)| \cos \left(s\omega t - \frac{2p\pi}{Qr} k \right) \quad (4.2)$$

Where:

- Q_R is the number of the rotor bars;
- k is the considered rotor bar;
- s the fundamental slip.


Figure 4.1: Squirrel Cage Rotor

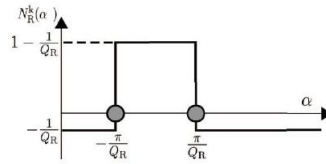
4.2 A winding function approach

As explained in [13], the winding functions of multi-turn coils placed in the cages are defined by:

$$N(\alpha_s) = \begin{cases} N_{turns} \cdot \left(1 - \frac{\tau}{2\pi}\right), & \alpha_1 \leq \alpha_s \leq \alpha_2 \\ -N_{turns} \cdot \frac{\tau}{2\pi}, & \text{rest of } \alpha_s \end{cases} \quad (4.3)$$

Where N_{turns} is the number of turns, τ is the coil pitch $\tau = \alpha_2 - \alpha_1$.

Two near-by bars and ring segments between them make the rotor loop (Figure 4.2). The rotor loop can be observed as one-turn coil with pitch $\tau = \frac{2\pi}{Q_r}$, where Q_r is the number of rotor bars. The winding function of the rotor loop 1, whose magnetic axis is in the centre of the reference frame fixed to the rotor, is given by Equation 4.4.


Figure 4.2: Rotor MMF: a winding function approach

$$N_{loop}(\theta_r) = \begin{cases} \left(1 - \frac{1}{Q_r}\right), & -\frac{\pi}{Q_r} \leq \theta_r \leq \frac{\pi}{Q_r} \\ -\frac{1}{Q_r}, & \text{rest of } \theta_r \end{cases} \quad (4.4)$$

This procedure may be apply to any number of bars Q_r .

In parallel with the calculation of the stator magnetomotive force, the analytical results were compared with those of the finite element software. Also in this case, simplifying assumptions were made about the design and feeding conditions. The case analysed in Section 4.4 concerns a squirrel cage rotor with twelve bars. With respect to this example, the winding functions of the first 4 loops of a 12-bars squirrel cage rotor are shown in the Figure 4.3. It is assumed that the rotor reference axis coincides with the 0 of the air-gap position.

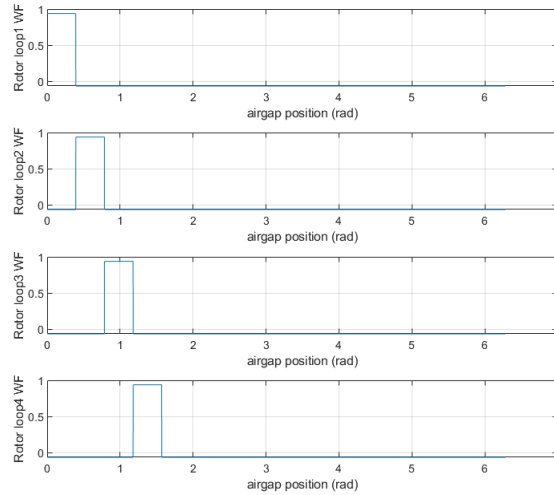


Figure 4.3: Winding functions of 4 loops (12 cages rotor)

4.3 Winding Theory - Ratio between Stator and Rotor

To simplify the study of the asynchronous motor, it was assumed, throughout the previous pages, that all rotor quantities are referred to the stator windings. According to this hypothesis, it was possible to derive the T-equivalent circuit model to study the Induction Motor at steady state (Section 1.5), as well as the d,q-equivalent circuit (Section 2.3) where d,q are reference axes rotating axes at an arbitrary speed. In the previous treatment, in fact, both the electrical and magnetic quantities and the equivalent circuit parameters were scaled by an appropriate ratio, defined in function to the number of equivalent stator and rotor windings. In order to estimate the rotor magneto-motive force and the magnetic field in the air gap, a similar (but inverse) operation to that mentioned above must be

performed. In fact, it will be necessary to return to the rotor the quantities referred to the stator windings first.

In accordance with [14], the following equation is used to estimate the value of the rotor current, after knowledge of the motor design choices. The postulate states that: the rotor current referred to stator (i.e. that flows in it) should produce the same magnetomotive's fundamental created by the rotor currents in the Q_R bars of the cage.

$$A'_{R,fundamental} = \frac{3}{2} q z_C \cdot K_{w,1} \cdot I'_R = \frac{Z_2}{p} \cdot \frac{1}{2\pi} \cdot I_R = A_{R,fundamental} \quad (4.5)$$

Where:

- q = Number of slots per pole per phase;
- z_C = number of conductors in series per slot;
- $Z_2 = Q_R$ number of rotor bars

And:

$$q z_C = \frac{Z_f}{2p} = \frac{N_1}{p} \quad (4.6)$$

Where:

- Z_f = number of conductors in series per phase, $Z_f = 2N_1$;
- N_1 = number of turns in series per phase

And N_1 is obtain through the following expression:

$$N_1 = p \cdot q \cdot \left[\frac{\{\text{nb. of conductors in the slot}\}}{\{\text{nb. of internal parallel paths}\} \cdot \{\text{nb. of external parallel paths}\}} \right] \quad (4.7)$$

From Equation 4.5, explicit the dependency between I'_R and I_R :

$$I'_R = \frac{Q_R}{3 \cdot Z_f \cdot K_{w,1}} \cdot I_R \quad (4.8)$$

and $K_{w,1}$ is the winding factor for the fundamental harmonic [15] of the magnetic flux density, obtained as:

$$K_{w,1} = k_{p1} \cdot k_{d1} \quad (4.9)$$

Where:

- k_{p1} is the pitch factor: $k_{p1} = \sin\left(\frac{\beta\pi}{2}\right)$ and $\beta = \frac{w_c}{\tau}$ is the coil pitch-to-pole pitch ratio (w_c is the coil pitch and τ is the pole pitch).
- k_{d1} is the distribution factor: $k_{d1} = \frac{\sin\left(\frac{\pi}{2m}\right)}{q \cdot \sin\left(\frac{\pi}{2mq}\right)}$; In this expression m is the number of stator phases, $q = \frac{N_{\text{slots}}}{m \cdot 2p}$ is the number of slots per pole per phase.

4.4 Testing the Rotor MMF

To validate the model, the analytical Rotor magnetomotive force, computed as described in Equation 4.1 should be compared with the Finite Element analysis results.

In order to isolate the contribution of the rotor magnetomotive force, some modification in the induction machine design should be done, as well as some choices in PC-FEA settings (Figure 4.4).

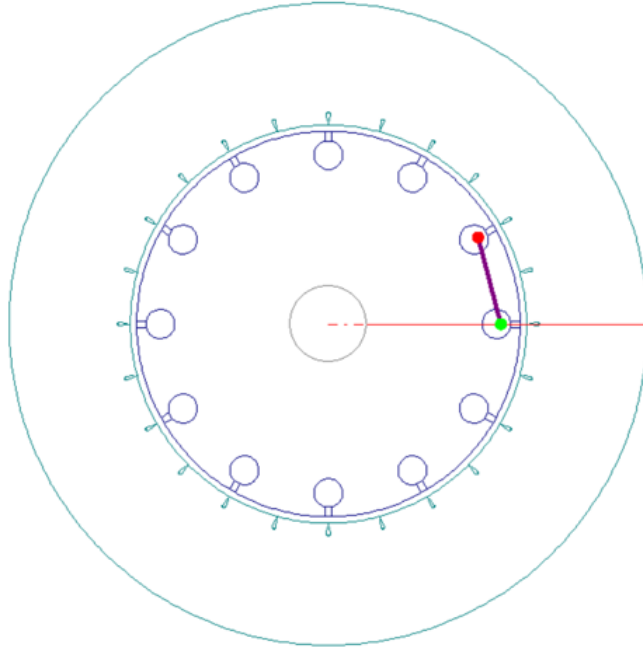


Figure 4.4: Simplified Geometry: Testing Rotor MMF

The most important assumptions made to compare FE with analytical results are the following:

- Assumption 1: *"The effect of slot openings is negligible and the air-gap depth can be considered constant and equal to the minimum distance between stator*

and rotor teeth".

Stator slot openings are set to be equal to the minimum allowed by the design software SPEED. Rotor slots are closed.

- Assumption 2: *The rotor is powered independently to the stator.*

Because in the design software PC-IMD it is not possible to remove the stator, it is assumed that zero current flows in the slots and that stator windings occupy a minimum area.

- Assumption 3: *Iron permeability is assumed to be infinite.*

The machine works under the hypothesis of magnetic linearity. The imposed current flowing in the rotor bars is chosen sufficiently low to avoid to see the effect of yokes and teeth magnetic saturation.

A single load point finite element analysis is performed in PC-FEA. A 12-bars squirrel cage rotor is considered. In this example, rotor reference axis is placed on the zero position of α_s (axis fixed to the stator). Stator current amplitude is set to zero, rotor current amplitude to 10 A (peak value), and $\theta = \omega \cdot t = 0$. Figure ?? shows the comparison between FEA and analytical results. The same procedure is repeated for different rotor positions (Figure 4.6), values of θ and motor designs.

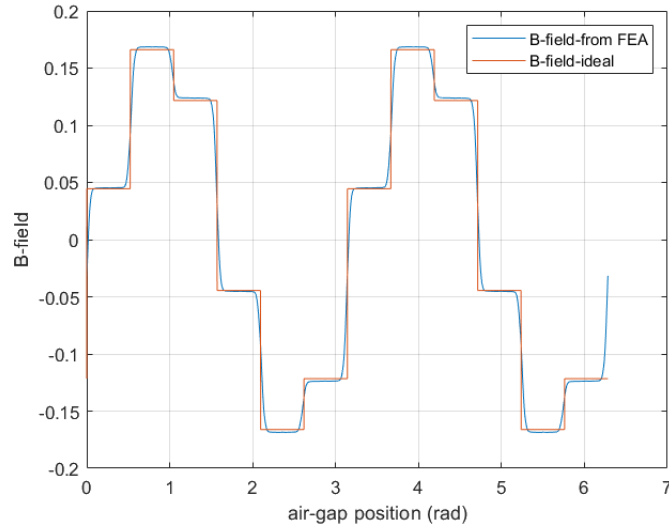
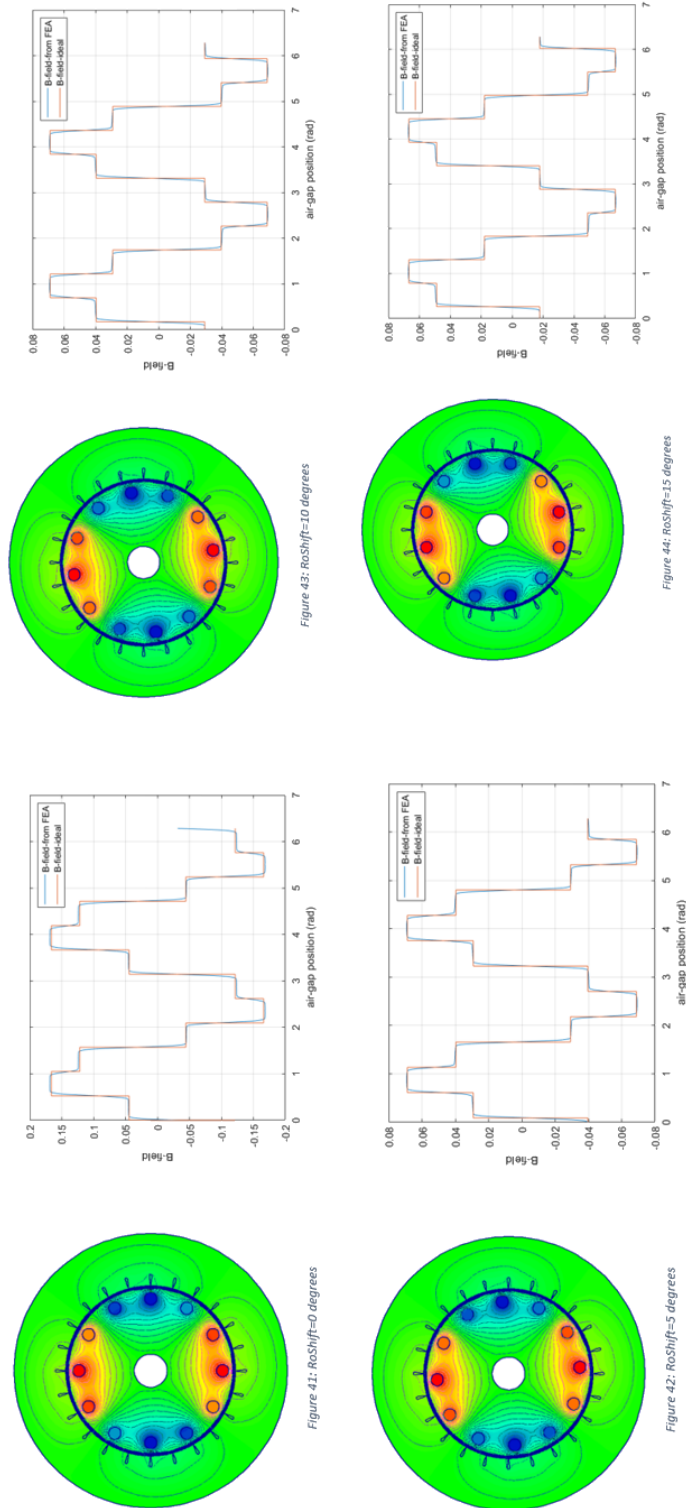


Figure 4.5: Comparison between FEA and analytical results



46
Figure 4.6: Comparison between FEA and analytical results: Different rotor positions

Chapter 5

Airgap Permeance

This work aims to a dynamical evaluation of radial forces in the air-gap. As discussed in Chapter 3 and 4, knowing the values of stator and rotor currents, together with the rotor position and design choices, the model will be able to evaluate the magnetomotive forces in the air-gap during a dynamic simulation. The magnetomotive forces' formulation was validated by comparing the analytical magnetic induction with Finite Element analysis results. In that case, the geometry of the induction motor and the value of currents injected in the stator and in the rotor were chosen in order to satisfy the following assumption:

- *Slotting Effect can be neglected:*
the air-gap width is set to its minimum value.
- *The machine work in magnetic linearity conditions:*
the effect yokes and teeth saturation can be neglected.

Accordingly to this hypothesis, the air-gap Permeance was defined as:

$$\Lambda_{\text{air}} = \frac{\mu_0}{\delta_{\text{airgap}}} \quad (5.1)$$

And the radial magnetic induction was computed as follows:

$$B_{r,\text{airgap}} = (A_s(\alpha, t) + A_R(\alpha, t)) \cdot \Lambda_{\text{airgap}} \quad (5.2)$$

Choosing an operating point interested by a relative small value of stator and rotor current, to avoid the machine working in a saturation zone, the air-gap magnetic induction (due to the contribution of both stator and rotor) computed analytically is compared with Finite Element Analysis results. Figure 5.1 shows the comparison discussed for Kyburz eRod IM design, at rated power (Section 1.4.3).

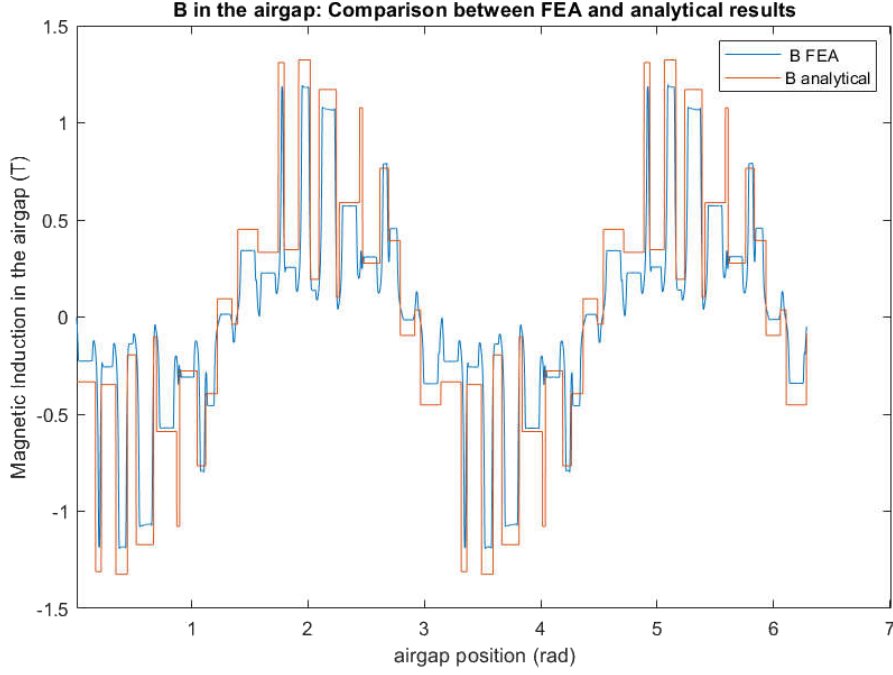


Figure 5.1: B-field with Ideal Permeance

In reality, however, the air-gap permeance is not a constant. Instead, it depends on the rotor position and on the operating point (i.e. stator currents amplitude). Therefore it is necessary to correct the equation of magnetic induction mentioned above with the following one, that takes into account this dependence.

$$B_{r,\text{airgap}} = (A_s(\alpha, t) + A_R(\alpha, t)) \cdot \Lambda_{\text{airgap}}(\alpha, t) \quad (5.3)$$

To take into account the presence of slots and the effect of yokes and teeth saturation, the expression of air-gap permeance should be corrected as follows [16]:

$$\Lambda_{\text{air}}(t, \alpha) = \frac{\mu_0}{g_{\text{air}}(t, \alpha) \cdot k_{\text{sat}}(t)} \quad (5.4)$$

Where $g_{\text{air}}(t, \alpha)$ is model the increasing of the air-gap width due to the presence of the slots, while $k_{\text{sat}}(t)$ is a function that describes the effect of saturation on the air-gap permeance.

5.1 Slotting Effect

5.1.1 Modified Air-gap width

In the computation of the ideal permeance, the air-gap depth was considered constant and equal to its minimum value (minimum distance between stator and rotor teeth). The aim of this section is to build a function $g_{air}(t, \alpha)$ that takes into account the presence of stator and rotor slots ([12] and [16]). A modified air-gap depth g_{air} is defined as follows:

$$g_{air}(t, \alpha) = \delta_{airgap} + e_s f_s(\alpha) + e_r f_r(t, \alpha) \quad (5.5)$$

Where:

- e_s is the stator entering ratio;
- $f_s(\alpha)$ is the stator slotting function;
- e_r is the rotor entering ratio;
- $f_r(\alpha, t)$ is the rotor slotting function.

The values of the entering ratio e_s and e_r depend only on the slot openings. The entering ratios are defined as suggested in [16]: $e_s = b_s/5$ and $e_r = b_r/5$, where b_s is the stator slot openings depth and b_r is the rotor slot openings depth (equal to zero for closed slots).

Figure 5.3 and Equation 5.6 show how stator slotting function has been defined with the help of a sinusoidal function:

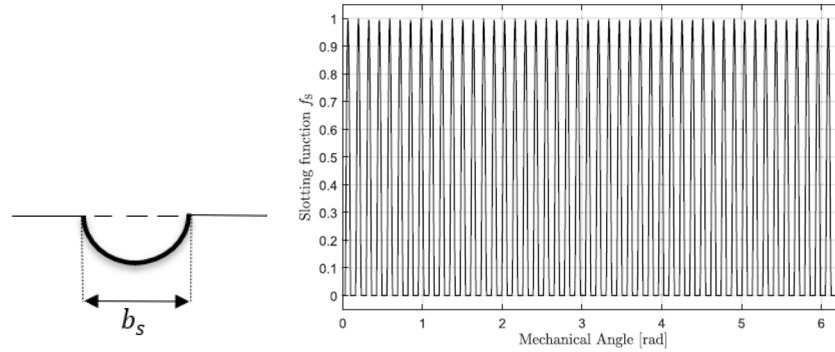


Figure 5.2: Computation of stator slotting function

$$f_s(\alpha_s) = \begin{cases} \frac{1}{1-h_{shift}} \sin(Q_S \alpha_s) - h_{shift}, & \text{for } -\frac{b_s}{2} \leq \alpha_s \leq \frac{b_s}{2} \\ 0, & \text{rest of } \alpha_s \end{cases} \quad (5.6)$$

Where:

- Q_s is equal to the number of stator slots;
- h_{shift} is an adjustment value calculated by comparing analytical with FE results. It is obtained by a simple optimisation routine that minimise the relative error between the two approach.

A similar procedure is repeated for the rotor slotting function. It should be underlined, that it depends not only on the air-gap position α_s , but also on time. This dependency is motivated with the fact that the rotor is rotating, and f_r will moves coherently with it. So the modified air-gap depth $g_{air}(t, \alpha_s)$ will change its distribution in the gap, accordingly with time (i.e. rotor position).

Figure 5.3 shows the modified air-gap depth for a particular time instant. The contribution of both stator and rotor slots is underlined. The resultant effect will be obtained by summing up the two contributions. Moreover, in Figure 5.3 it is clearly visible, how the effect of the slots creates a deviation from the ideal thickness.

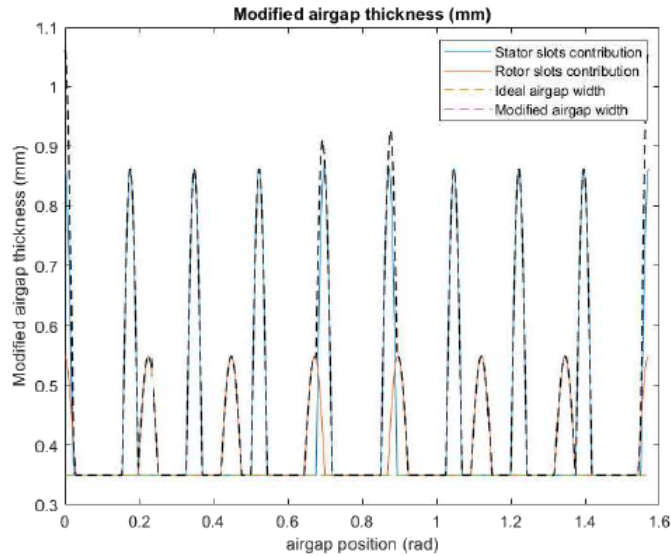


Figure 5.3: Modified air-gap depth

Once the modified air-gap depth is defined, it is possible to include the slotting effect into the air-gap permeance formulation. It will be modified as follows:

$$\Lambda_{air} = \frac{\mu_0}{g_{air}(t, \alpha)} ?? \quad (5.7)$$

The air-gap permeance, in a certain time instant, will appear as shown in Figure

5.4. Its value deviate from the ideal Λ_{airgap} : a reduction may be notices in correspondence of stator and rotor slots.

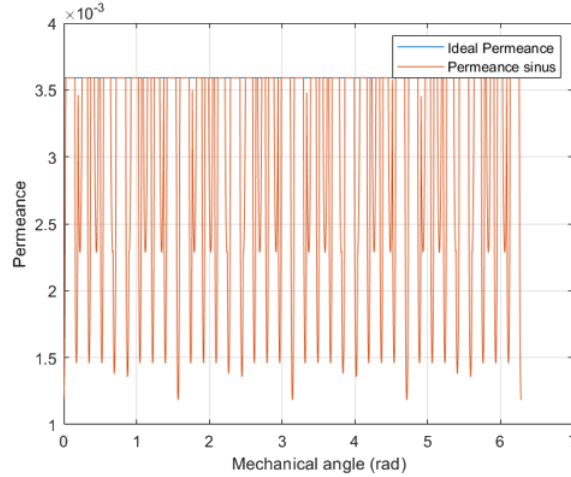


Figure 5.4: Air-gap Permeance - Including slotting effect

Using an expression of permeance that includes slotting effect (Equation ??), radial magnetic induction is computed analytically. In Figure 5.5, a comparison between analytical and PC-FEA results is show. Also, in that case, the hypothesis to work in magnetic linearity is considered to be valid (the operating points are chosen at relatively low currents). As described in Chapter 3 and 4, a single load point finite element analysis is performed in PC-FEA. Stator and rotor currents amplitude and phase together with rotor position are specified in GoFER. Same inputs are imposed to the system-level model.

5.2 Saturation

The aim of this section is to include, in the expression of the air-gap permeance and of the radial magnetic field, the contribution of the teeth and yokes saturation. Different approaches are described in literature. However, they appear to be imprecise and difficult to implement in practice. In this work it has been chosen to model the effect of magnetic saturation by integrating finite element software results into the analytical model. The initial idea was to study the stator and rotor separately. The magnetic field results obtained analytically and with PC-FEA for a wide range of currents were compared.

It is assumed to have validated the approach used by the analytical model to

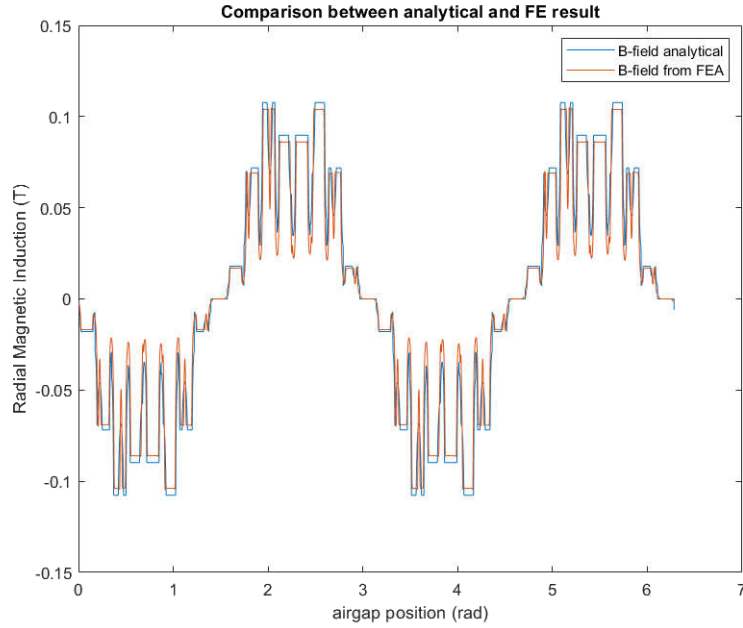


Figure 5.5: Radial Magnetic Inductance - Including slotting effect

calculate the magneto-motive forces and to have correctly modelled the presence of slots with the help of sinusoidal functions (Chapter 3, 4, 5.1). If these assumptions are met, the magnetic induction calculated analytically and with the PC-FEA software will differ only by a proportion related to saturation.

The idea is to isolate this proportion and to analyse how the effect of saturation impacts on air-gap permeance, decomposing this term into its spatial harmonics. As mentioned above, the stator and rotor are considered separately. The idea developed here is based on the construction of a virtual permeance, defined as the ratio between the magnetic induction calculated by finite element software PC-FEA and the magnetomotive force of the stator (since only the effect due to the stator is being considered and a null current is imposed in the rotor), as shown in Figure 5.6. This is repeated over a wide range of stator current amplitude. Following this procedure, the virtual air-gap permeance is computed (Figure 5.7). It is interesting to notice that the permeance is decreased, if compared to Figure 5.4 not only of a constant value. In fact, it is clearly visible that permeance is suffers by the effect of higher order harmonics.

It would be possible to observe the contribution of permeance harmonics related to their spatial frequency and store those data into a Look Up Table (LUT). Entering the value of stator current, into the LUT will be selected a function $k_{sat}(I)$ that

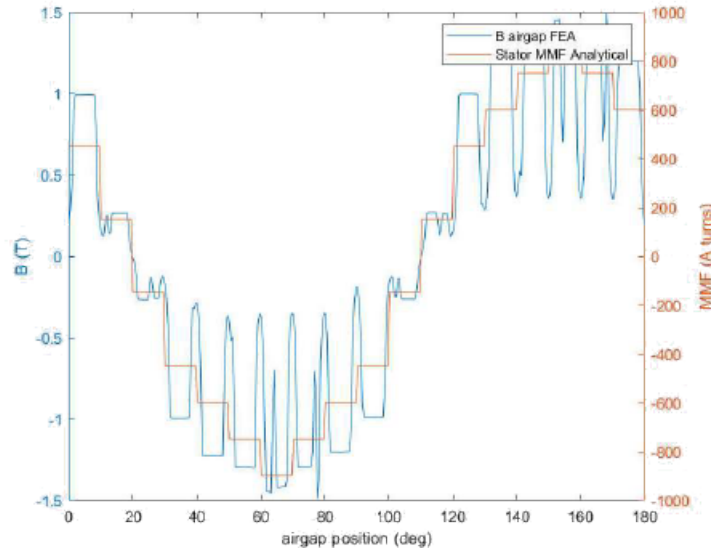


Figure 5.6: Comparison between PC-FEA Magnetic Induction and Stator Magnetomotive Force computed analytically, for a defined value of stator current amplitude

describes what is the contribution due to saturation to the air-gap permeance. For reason of time, this approach has not been developed. But to take saturation into account, coefficients have been defined, which reduce the permeance by a constant value. This constant is equal to the ratio between the ideal permeance and the dc value of the virtual permeance. The formulation of the Air-gap permeance will be modified as follows:

$$\Lambda_{\text{air}}(t, \alpha) = \frac{\mu_0}{g_{\text{air}}(t, \alpha) \cdot K_0(I)} \quad (5.8)$$

The saturation constant obtained in this way is what would have been obtained by comparing the FFT (Fast Fourier Transformation) amplitudes of the first spatial harmonic of Ideal and Virtual Permeance (at 0 hz).

Figure 5.8 shows the saturation coefficients K_0 obtained by evaluating, for the same range of currents, the effect of stator only and of rotor only. This approach is conceptually wrong. It is not correct to decouple the two effects and the superimpose them, while studying saturation.

In order to use the same idea (only one constant coefficient, that reduce the permeance) it is needed to perform finite element analysis for real operating points. Scripting in SPEED the calculation of stator and rotor current values for real operating points (i.e. varying the imposed rotor speed or load torque), it will

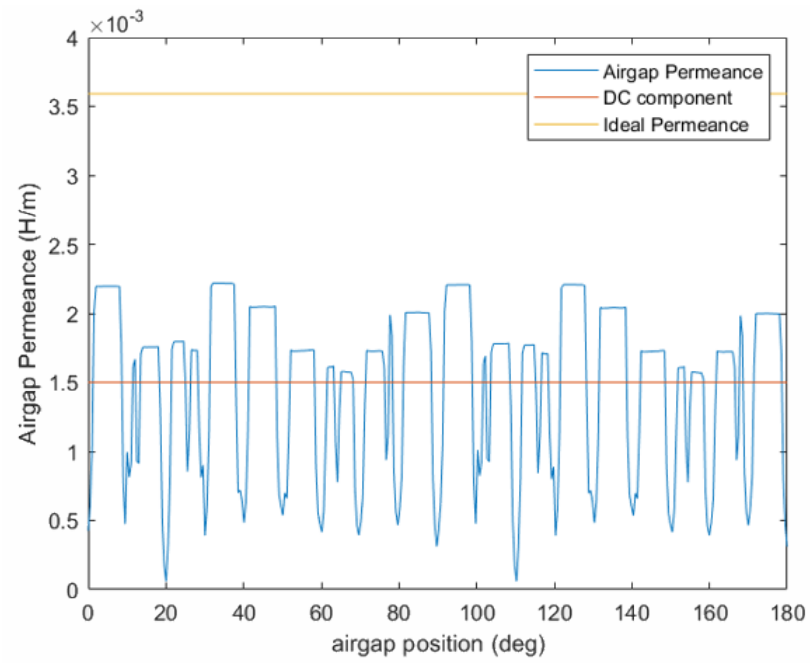


Figure 5.7: Virtual Permeance

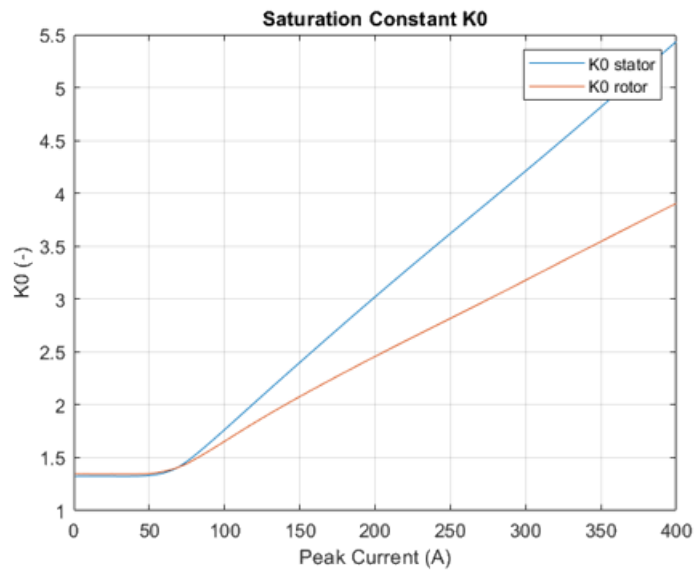


Figure 5.8: Saturation Constant

possible to collect FEA results for all the operating range of the Induction motor. Using the same inputs in the analytical model (i.e. varying the imposed rotor speed or load torque in Simulink environment) the analytical radial magnetic induction is computed for the same operating points of FE solver. Using a permeance that includes the effect of slots, the Magnetic Induction computed analytically and by PC-FEA will differ only of the proportion related to saturation.

Chapter 6

Noise and Vibrations

6.1 Noise App: Introduction

Noise App is a Python-based application developed by the department of Engineering Service of Siemens SW Leuven. Knowing the distribution of radial Maxwell stress tensor in the air-gap, Noise App is able to perform structural and acoustic analysis on a electrical machine stator (Figure 6.1). For which concerns structural analysis, it uses a 2D ring model. The vibration displacement is calculated on a point of stator surface. Regarding the estimation of acoustic pressure, the electrical machine is approximated with a 3D infinite cylinder. The acoustic pressure is computes at one meter far from the machine axis [17].

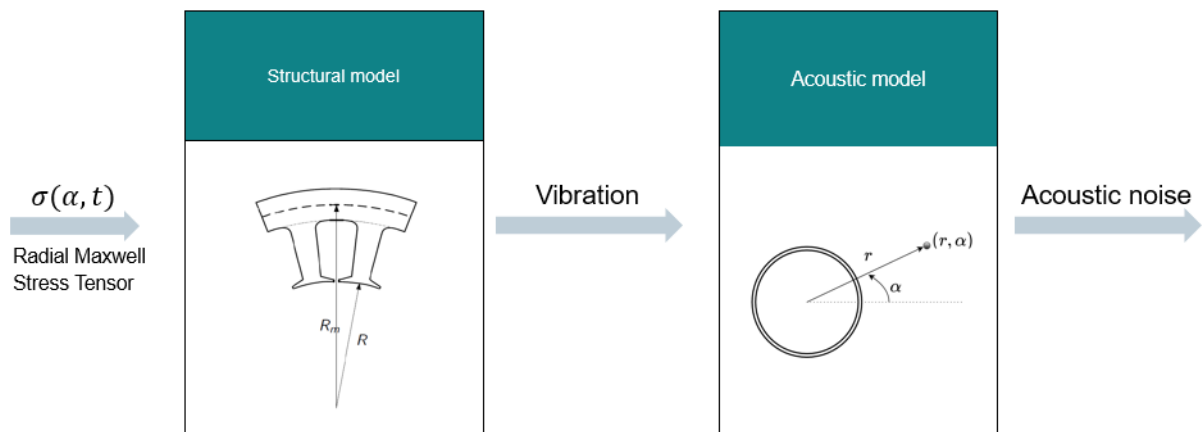


Figure 6.1: Structural and acoustic model- Noise App

Noise App results are shown in the following two sections. Two different cases are analysed:

- The mechanical speed is fixed. After a transient, the rotor is rotating at the desired speed. The machine is working at steady state. The data used for this test concerns the variation of the magnetic induction distribution during one complete mechanical rotation.
- Run-Up test: during the entire simulation the imposed mechanical speed is constantly varied (for example from 0 to synchronous speed in Δt). In this way it is possible to observe, in a wide range, which operating points (i.e. which frequency) are related to bigger NVH issues.

6.2 Noise App Inputs

Noise App receives as input, from the system-level model, the distribution of forces in the air-gap.

Forces are computed using Maxwell stress tensor. Since it is assumed to be the main responsible to the NVH, only the radial component is considered. Radial Maxwell stress tensor is computed as follows [17]:

$$\sigma(\alpha, t) = \frac{B_{r, \text{airgap}}^2}{2\mu_0} [\text{N/m}^2] \quad (6.1)$$

Radial magnetic induction has been computed using the system-level model of the induction machine discussed throughout these pages. Figure 6.2 shows the distribution of magnetic induction during one complete mechanical rotation of the rotor (x-axis is the air-gap position $0 < \alpha_S < 2\pi$, y-axis is the time needed for a complete rotation $0 < t < 15$ ms). In this example, the Kyburz eRod is running at steady state at rated power.

Figure 6.3 shows the distribution of radial forces in the air-gap for one complete mechanical rotation (Kyburz eRod IM design, Section 1.4.3, at steady state). It is computed accordingly to Equation 6.1.

Figure 6.4 the distribution of Maxwell stress tensor for the first time instant considered in the simulation, $t = t_0$.

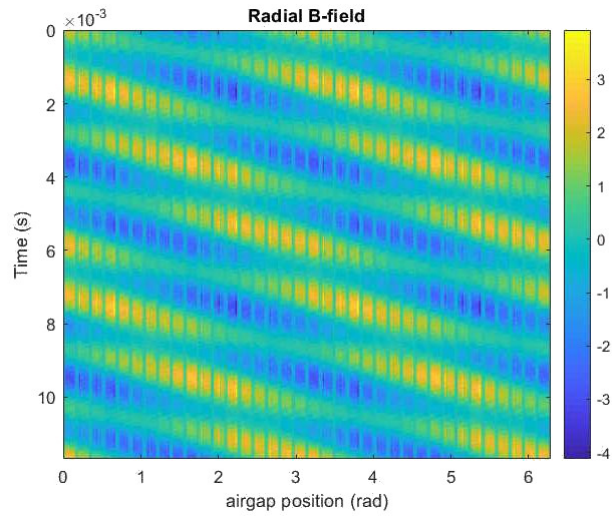


Figure 6.2: Radial Magnetic induction: air-gap distribution during a complete mechanical rotation

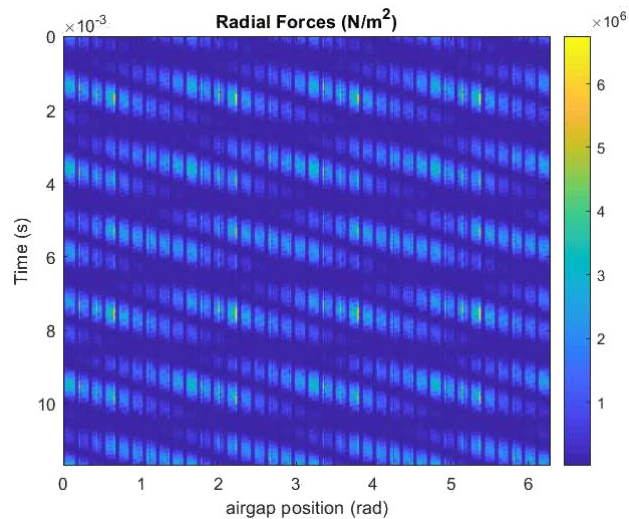


Figure 6.3: Maxwell stress-tensor: air-gap distribution during a complete mechanical rotation

6.3 Results: Constant RPM simulation

This section shows Noise App results for a simulation conducted at constant rotor speed. It was considered that the induction machine is at steady state and the

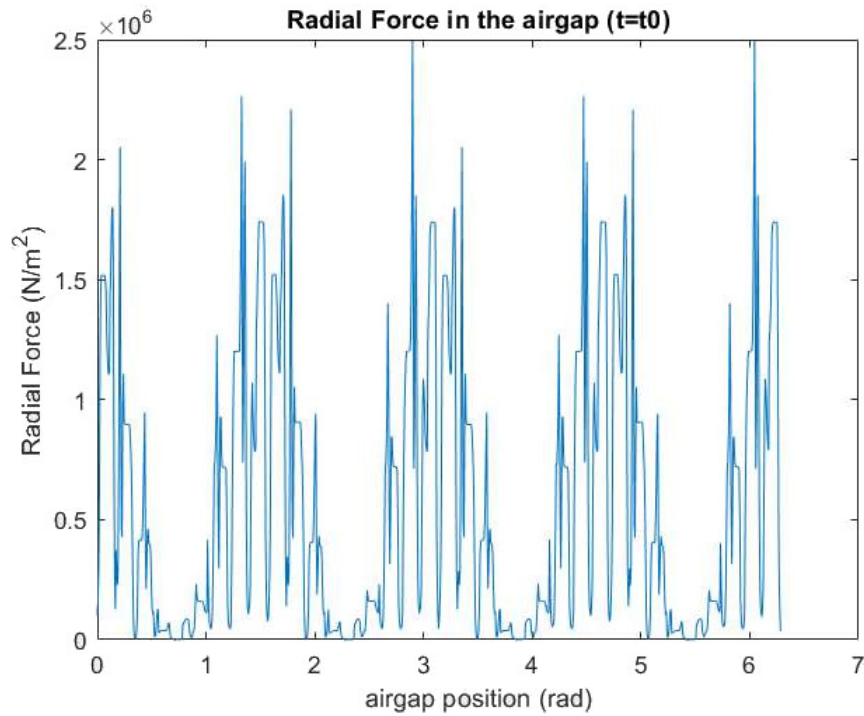


Figure 6.4: Maxwell stress-tensor distribution in the airgap

data of air-gap radial forces that were analysed concerns one complete mechanical rotation.

The results refer to Kyburz eRod IM design (Section 1.4.3). The simulation is conducted at motor rated power:

- Rotor mechanical speed $\Omega = 5140$ rpm;
- Frequency $f = 176$ Kz;
- RMS value of stator current $I_{s_{rms}} = 136$ A.

Table 6.1 shows the results of the structural analysis.

Figure ?? shows the vibration displacement and sound pressure versus frequency. Referring to Table 6.1 it possible to notice that in particular, mode 4th has a big impact in both vibration displacement and sound pressure. In Figure ?? the effect of mode 4th is clearly visible. At a frequency of 6825.5 Hz, vibration and noise distributions present a peak.

The air-gap forces have been computed both including and neglecting the effect of material saturation in the air-gap permeance expression. In Figure ?? it is

Mode order	Eigenfrequency [Hz]
0	8606.3
1	11529.2
2	1495.4
3	3910.7
4	6825.5
5	9987.8

Table 6.1: Noise App results: Mode and Frequencies

clearly visible that There are shown the results for both saturated and not saturated case. It is clear that considering the effect of saturation is not a minor aspect.

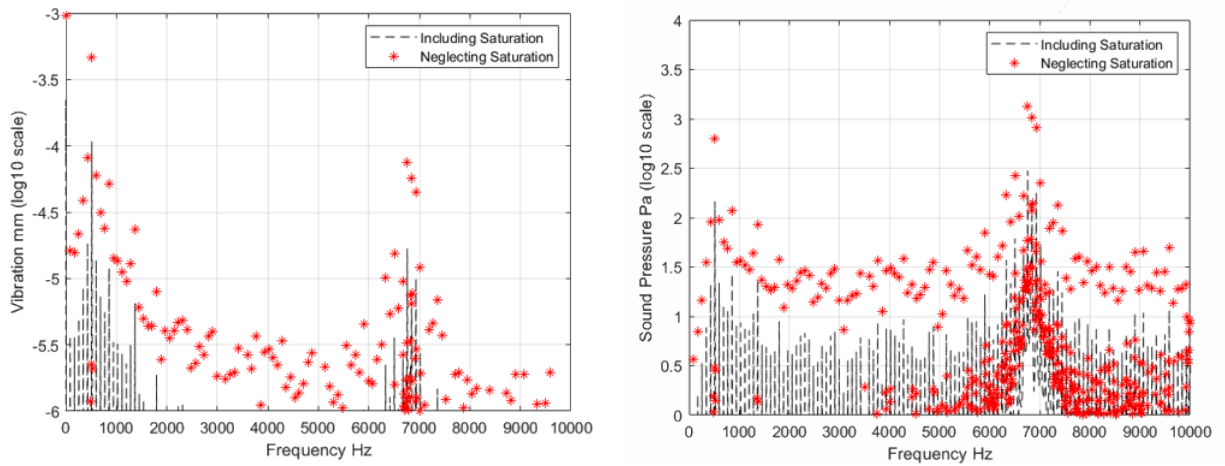


Figure 6.5: Noise App results: Constant RPM simulation. Left: Vibration displacement vs. frequency. Right: Sound Pressure vs. frequency

6.4 Run-Up Results

Run-Up test was conducted with:

- Rotor speed is varied between 1000 and 5000 rpm;
- Id and Iq references imposed via current controller (fixed values)

Spectrograms in Figure 6.6 show Noise App results related to the Run-Up simulation. Note that the amplitude of Power (dB) is quite different if saturation is neglected or included. In spectrograms significant time-orders are shown. Kyburts eRod IM, as designed in Section 1.4.3 presents a structural resonance at a frequency equal to 10.001 Hz.

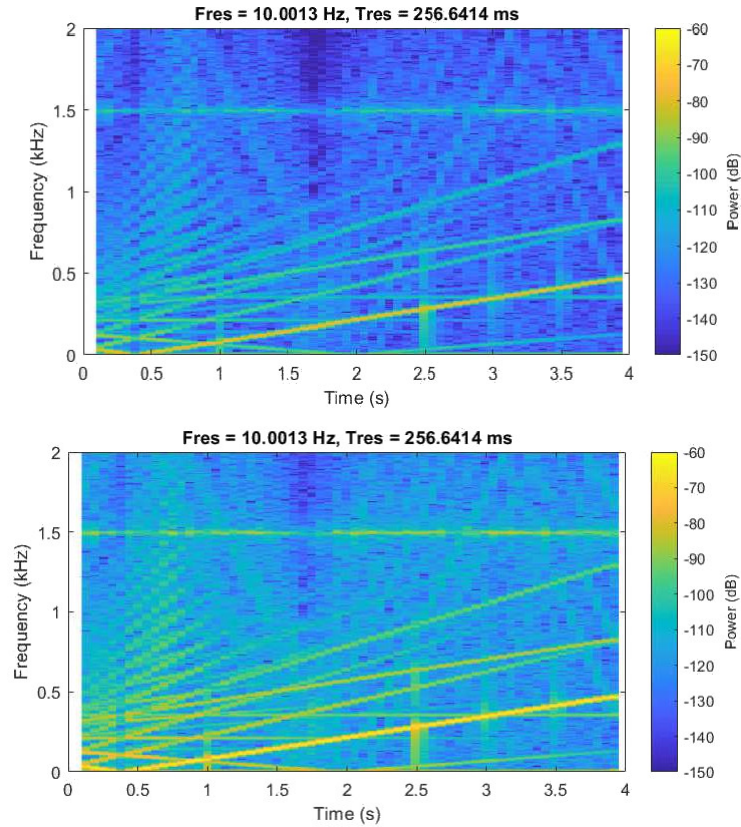


Figure 6.6: Noise App results: Run-Up test. (Up) Result obtained including saturation effect in air-gap permeance computation. (Down) Result obtained neglecting saturation effect in air-gap permeance computation.

Chapter 7

Conclusions

In this work, a fast induction machine system-level model able to capture spatial force effect is discussed. It is based on 2-D machine geometry (skewing is neglected) and material characteristics. The model includes the effect of machine harmonics due to winding distribution, slotting and saturation. The IM model is constructed using the early-stage machine-design Simcenter SPEED, by a fast, semi-analytical parameter extraction approach.

This thesis tries to provide a useful tool for electric motor design. The coupling with the Python-based application *Noise App* allows to a fast prediction of the NVH characteristics of the electrical drive.

The model is not to be considered ready to be used in the design phase. As described in Section 5.2, the effect of saturation is not properly taken into account and the *Noise App* results (Section 6 are very different from what is expected in reality. One point that definitely needs to be strengthened is increasing the nonlinear accuracy of the system-level model. Moreover a bigger integration of the system-level model with Finite Element results will benefit the precision.

The examples discussed in this work refers to Kyburz eRod IM (Section 1.4.3). The machine data are to be considered extremely indicative . Assuming that the data related to the motor design are fully known, it would be interesting to validate the entire process comparing simulation results with real measurements. The overall model may be validated through vibration measurements.

Bibliography

- [1] G. Pellegrino, A. Vagati, B. Boazzo, and P. Guglielmi. Comparison of induction and pm synchronous motor drives for ev application including design examples. *IEEE Transactions on Industry Applications*, 48(6):2322–2332, 2012.
- [2] B. Sarlioglu, C. T. Morris, D. Han, and S. Li. Benchmarking of electric and hybrid vehicle electric machines, power electronics, and batteries. In *2015 Intl Aegean Conference on Electrical Machines Power Electronics (ACEMP), 2015 Intl Conference on Optimization of Electrical Electronic Equipment (OPTIM) 2015 Intl Symposium on Advanced Electromechanical Motion Systems (ELECTROMOTION)*, pages 519–526, 2015.
- [3] Optimization of scalable realtime models and functional testing for e-drive concepts. <https://cordis.europa.eu/project/id/769506/it>. Accessed: 2020-07-3.
- [4] Siemens PLM Software. *Simcenter SPEED: PC-IMD user’s manual*.
- [5] Siemens PLM Software. *Simcenter SPEED: PC-FEA user’s manual*.
- [6] Siemens PLM Software. *Simcenter SPEED: PC-IMD GoFER user’s manual*.
- [7] *Symmetrical Induction Machines*, chapter 6, pages 215–270. John Wiley Sons, Ltd, 2013.
- [8] A. Cavagnino. *Macchine elettriche ii, parte di dinamica delle macchine elettriche*, 2018.
- [9] P. Pillay R.J. Lee and R.G Harley. D,q reference frames for the simulation of induction motor. *Electric power system research*.
- [10] Siemens PLM Software. Simcenter amesim: Electrical machine drives library.
- [11] Jan Otýpka, Petr Orsag, Vítězslav Stýskala, Dmitrii Kolosov, Stanislav Kocman, and Feodor Vainstein. The enlarged d-q model of induction motor with the iron loss and saturation effect of magnetizing and leakage inductance. 423:11–22, 01 2016.
- [12] W. M. Bischof, M. D. Hennen, and R. M. Kennel. Synthesized magnetic flux density in three-phase cage induction machines with matlab simulink. In *2015 18th International Conference on Electrical Machines and Systems (ICEMS)*, pages 109–115, 2015.
- [13] G Joksimovic, M Djurovic, and J Penman. Cage rotor mmf: winding function

- approach. *IEEE Power Engineering Review*, 21(4):64–66, 2001.
- [14] A. Cavagnino. *Macchine elettriche ii, parte di costruzioni elettromeccaniche*, 2018.
- [15] Jacek F Gieras, Chong Wang, and Joseph Cho Lai. *Noise of polyphase electric motors*. CRC press, 2018.
- [16] Jean Le Besnerais. *Reduction of magnetic noise in PWM-supplied induction machines-low-noise design rules and multi-objective optimization*. PhD thesis, 2008.
- [17] Gustavo Myrria, Fabien Chauvicourt, and Cassio Faria. Fast computation of the acoustic response of electrical machines via analytical means. 09 2016.